

Current-induced magnetization switching in small domains of different anisotropies

Ya. B. Bazaliy

Argonne National Laboratory, Material Science Division, 9700 S. Cass Avenue, Argonne, Illinois 60439, USA

B. A. Jones

IBM Almaden Research Center, 650 Hary Road, San Jose, California 95120, USA

Shou-Cheng Zhang

Department of Physics, Stanford University, Stanford, California 94305, USA

(Received 29 August 2003; published 22 March 2004)

Several recent experimental studies have confirmed the possibility of switching the magnetization direction in small magnetic domains by pumping large spin-polarized currents through them. On the basis of equations proposed by Slonczewski for domains with uniform magnetization, we analyze the stability and switching in two cases which differ by the anisotropy type. One of anisotropy types corresponds to that of the existing experimental device. Qualitatively different behavior is found in shapes of bistable regions and regions with stable precession. Stabilization of unusual “canted” equilibria is found in one of the cases. The sensitivity of the switching pattern to a change in anisotropy pattern underscores the necessity of theoretical guidance for the interpretation of experimental results. We propose experiments to search for stabilized canted equilibria and precession cycles. Our study is analytic as opposed to recent numeric work and the method can be applied to other anisotropy patterns as the experimental interest develops.

DOI: 10.1103/PhysRevB.69.094421

PACS number(s): 75.60.Jk, 72.25.-b, 85.75.-d, 72.15.Gd

I. INTRODUCTION

Currently considerable experimental interest^{1–23} is devoted to the torques created by spin-polarized currents in a magnet. This interest is in part fueled by the proposals of developing a convenient writing process for the magnetic nonvolatile random access memory where the reading process will be based on the magnetoresistance effect.²⁴ A general theoretical framework for the description of such “spin-transfer” torques is set in Refs. 25–27. The spin-transfer effect is the nonequilibrium interaction induced by the electric current I flowing between two metallic ferromagnets separated by a normal metal spacer. This interaction is qualitatively different from the Ruderman-Kittel-Kasuya-Yosida exchange observed at $I=0$, and should also be distinguished from the interaction with the Oersted field of the current. Spin transfer is a subject of recent interest in the field of spintronics.

One of the particular experimental setups in which this effect can be studied is a thin (≈ 100 nm) normal metal wire (called a “pillar” in the papers of the Cornell group¹⁰) with two magnetic pieces embedded in it (see Fig. 1). If the distance between the magnetic pieces does not exceed the spin diffusion length l_{sd} in the normal spacer between them, and their magnetizations are noncollinear, a current passing through the wire will induce spin-transfer torques, arising from the interaction of electron spins polarized by one magnet with the magnetization of another magnet. Such a setup was originally considered by Slonczewski.²⁶ There it was assumed that both magnetic pieces are isotropic and that initially their magnetizations are not collinear. A counterintuitive prediction of Slonczewski²⁶ was that in the presence of the current both magnetizations will rotate in a fixed plane keeping the angle between them constant. This was called a

“windmill,” because the way in which longitudinal motion of the current is transformed into the rotational motion of the magnetization is quite similar to the way in which the longitudinal motion of wind is transformed into the rotational motion of the sails in the mechanical windmill.

The windmill effect was predicted in the framework of an assumption that there is no magnetic anisotropy in the pieces. However for the real material one must also take into account magnetic crystalline anisotropies and the interaction with the induced magnetic field (shape anisotropy). Clearly, anisotropy will work against a windmill effect by creating barriers to reversal. The magnetization motion thus becomes more complicated. The spin-transfer torque now leads to switching between the equilibrium directions defined by the strong anisotropy. Such switching results from the competition between the energy dissipation described by Gilbert damping coefficient and energy influx from the electron current described by spin-transfer torque. Switching happens when the current exceeds a critical value (determined by the anisotropies and applied external magnetic field), which gives potential for memory applications.

In this paper we summarize our work on the exact solutions of the dynamic equation with the spin-transfer term for

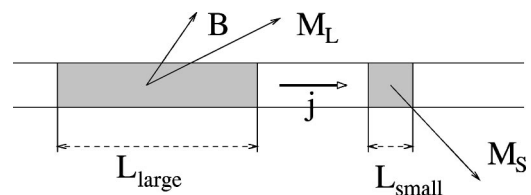


FIG. 1. Experimental setup. Current j is passed through a nano-wire with two magnetic pieces (shaded areas). External magnetic field B can be applied in an arbitrary direction.

several types of anisotropy. Our results were briefly reported in a series of short publications.^{28–30} There were other attempts to incorporate anisotropies including approximate treatments in earlier experimental reports.^{10,14} An extensive numeric treatment of a particular experimental situation was given by Sun.³¹ Later, a numerical calculation was used by Grollier *et al.*¹⁶ to find critical currents for a certain anisotropy. In contrast, our approach gives exact results and therefore can be very important for the comparison of experimental results and the spin-transfer theory.

Currently, experiments are performed with structures in which one of the magnetic pieces is much larger than the other. This brings a considerable simplification into the problem as follows. At a given current density j the spin-transfer torque T_{st} is proportional to the cross section of the wire. At the same time the torques T_a created by the anisotropy terms are proportional to the volume of the magnetic piece. Therefore the ratio $T_{st}/T_a \sim 1/L$, where L is the length of the piece, and the small piece will be affected by the spin-transfer torque starting from a much smaller value of j . One can therefore neglect the effect of T_{st} on the large piece, called a polarizer, and assume its magnetization to be constant. Torques on the small piece then occur from spin-polarized itinerant electrons coming into it either directly from the large piece or after multiple reflections between the pieces. Magnetizations of the large and small pieces will be denoted as \mathbf{M}_L and \mathbf{M}_S , respectively.

Our method of finding the switching diagram is as follows. We assume that the analyzer is in a single domain state and therefore its magnetization is described by the modified Landau-Lifshitz equation with spin-transfer term included.²⁶ For each (j, \mathbf{B}) point we find the equilibrium positions of \mathbf{M}_S and then analyze their stability exactly. Knowing the nature of each and all equilibria we can construct the topology of the time-evolution flow of \mathbf{M}_S (phase portrait) and predict qualitatively the overall behavior of the system. As the parameters change, the nature of some equilibria changes from stable to unstable, at which point the whole phase portrait changes. This is when the switching occurs. Sometimes neither of the equilibria is stable which implies the existence of stable cycles, because \mathbf{M}_S moves along the compact manifold (sphere). Such stable cycles were first considered for a particular setup³² and observed numerically.³¹ Due to energy dissipation they would be impossible without the current. However for $j \neq 0$ there is a constant supply of energy which feeds the periodic motion of \mathbf{M}_S .

To test the theory, one would like to be able to control the direction of the magnetization of the polarizer with respect to the anisotropy directions of the small piece. The easiest way to change \mathbf{M}_L is an application of the external magnetic field \mathbf{B} . Of course, \mathbf{B} will also act on the small piece and must be taken into account in the equations of motion. The properties of a system with a given anisotropy K_{ik} can ultimately be presented as a phase diagram in the four-dimensional space of parameters (j, \mathbf{B}) with spin-transfer effects determined by the magnitude of the current and by the direction of the spin polarizer $\mathbf{M}_L = \mathbf{M}_L(\mathbf{B})$. Different regions of such a diagram would correspond to different stable directions of \mathbf{M}_S . The boundaries between them will show where the small mag-

netic piece switches from orientation to the other; thus we will call it a “switching diagram.” In this paper we calculate a section of the full four-dimensional switching diagram for certain directions of \mathbf{B} and certain anisotropies. Our method can be applied to similar calculation for other directions of \mathbf{B} and other anisotropy tensors as the experimental need in them will arise.

Note that for technical applications in the memory writing process one is interested in finding anisotropy tensors which satisfy the following conditions: (a) there is a section of the phase diagram at a fixed external field \mathbf{B}_0 where \mathbf{M}_S is bistable at $j=0$; (b) the two metastable states differ in a property that is easy to measure, usually in their resistivity which depends on the angle between \mathbf{M}_S and \mathbf{M}_L ; (c) by passing a current one can switch back and forth between these two metastable states. However for the purposes of testing the theory of spin-transfer torques it is reasonable to start with the cases where the phase diagram is simplest, can be calculated exactly, and then compare theoretical and experimental results. We will discuss the structures considered in this paper in terms of their potential for application in memory devices in conclusion, Sec. V.

A current can also act on the magnetic pieces in a more conventional way through the magnetic field induced by the current (Oersted field). Such induced fields are always present, and their effect, used in existing technical applications,³³ can be much larger than that of electron spin transfer. However induced magnetic fields decrease as the size of the structure goes down and at sufficiently small size their effect will become negligible compared to the spin-transfer effect (see Appendix A).

If the size of the pieces is larger than the domain wall width, the magnetization may not be uniform throughout the piece. In this case continuous equations^{27,34} must be used inside each piece to determine the magnetic configuration. Our previous results²⁷ showed that for large current densities substantial deviations from the easy-axis direction can result at the interface, which heal in an oscillatory fashion into the bulk with a length scale comparable to the domain wall width. In the present paper we assume that the small magnetic piece is sufficiently smaller than the domain wall width in all directions, and treat it as magnetically uniform. Numeric studies of some nonuniform configurations were done in Refs. 35–37.

The paper is organized as follows. In Sec. II we discuss the modified Landau-Lifshitz equation with spin-transfer term, and describe how we find equilibria and analyze their stability. In Sec. III we discuss the “axial” anisotropy pattern for which the calculations are simpler, but which is more difficult to realize experimentally. The axial case is used as an example to introduce and discuss important concepts and approximations which we then use in Sec. IV to analyze the structure used in actual experiments of the Cornell group.¹⁰ In Sec. V we make conclusions and describe several subtleties that were ignored in the present paper but may be important in a real experiments and call for further work.

II. DYNAMIC EQUATION FOR THE SMALL PIECE

To write down the conventional Landau-Lifshitz equation we need to know the magnetic energy of the small piece. It is

given by a sum of intrinsic anisotropy term, shape anisotropy term, interaction with external magnetic field, and exchange interaction with the large piece. We approximate the shape of the small piece by an ellipsoid, so that the shape anisotropy is given by a demagnetization tensor N_{ik} :³⁸

$$\frac{F}{V} = \frac{1}{2}(-K_{ik}^{(intr)}n_in_k + 4\pi M_i N_{ik} M_k) - B_i M_i - J_{ex} S_i n_i, \quad (1)$$

where $M_i = M_{S_i}$ is the magnetization of the small piece, $K^{(intr)}$ is the intrinsic anisotropy tensor, and J_{ex} is the exchange coupling between the pieces across the spacer. Vectors \mathbf{n} and \mathbf{s} are unit vectors along the magnetization of the small and large pieces, respectively. According to Slonczewski,²⁶ the modified Landau-Lifshitz equation for \mathbf{M} has the form

$$\begin{aligned} \dot{\mathbf{M}} = & -\frac{\gamma}{V} \dot{\mathbf{L}} = \gamma \left[-\frac{\delta F}{\delta \mathbf{M}} \times \mathbf{M} \right] \\ & + \frac{\gamma \hbar}{V} \frac{j}{2} A \frac{j}{e} g(P, \mathbf{sn}) (\mathbf{n} \times [\mathbf{s} \times \mathbf{n}]) + \tilde{\alpha} [\mathbf{n} \times \dot{\mathbf{n}}], \end{aligned} \quad (2)$$

where $\gamma = g\mu_B/\hbar$ is the gyromagnetic ratio, V and A are the volume and cross-section area of the piece, $\tilde{\alpha}$ is the Gilbert damping coefficient, P is the degree of spin polarization of the electrons coming out of the large piece, and the spin polarization factor $g(P, \mathbf{sn})$ is given by

$$g(P, \mathbf{sn}) = \frac{1}{f(P)(3 + \mathbf{sn}) - 4}; \quad f(P) = \frac{(1+P)^3}{4P^{3/2}}. \quad (3)$$

The second term in Eq. (2) represents the spin-transfer torque. Details of the derivation can be found in Ref. 26. We would like to emphasize that calculation of the spin-polarization factor is a subject of many papers and the issue is not completely resolved at the present time. Its magnitude was investigated in different regimes as a function of the degree of spin polarization in the ferromagnets, properties of the boundaries, mean free path, and spin-relaxation lengths.³⁹⁻⁴⁵ Here we use the expression derived by Slonczewski.²⁶ It is generally true for all expressions of the spin-polarization factor that it is a growing function of the angle between \mathbf{s} and \mathbf{n} with maximum value reached for the antiparallel configuration. The physical meaning of such a behavior is rather simple: since it is harder to pump the current through the antiparallel configuration, the process generates more torque. For example, for a complete spin polarization the resistance of the antiparallel configuration is infinite and correspondingly $g(1, -1) = \infty$. Comparison with experiment can show how accurate were the assumptions made in Ref. 26 to derive g .

Equation (2) can be rewritten in terms of \mathbf{n}

$$\begin{aligned} \dot{\mathbf{n}} = & [(\vec{\omega}_H + \hat{\omega}_K \mathbf{n}) \times \mathbf{n}] + \omega_j g(P, \mathbf{sn}) [\mathbf{n} \times [\mathbf{s} \times \mathbf{n}]] + \alpha [\mathbf{n} \times \dot{\mathbf{n}}] \\ = & \mathbf{F}(\mathbf{n}) + \alpha [\mathbf{n} \times \dot{\mathbf{n}}] \end{aligned} \quad (4)$$

with rescaled coefficients

$$\begin{aligned} \vec{\omega}_h = & \gamma \left(\mathbf{B} + \frac{J_{ex}}{M} \mathbf{s} \right), \quad (\omega_K)_{ij} = \frac{\gamma}{M} (K_{ij}^{(intr)} - 4\pi M^2 N_{ij}) \\ \omega_j = & \frac{\gamma \hbar}{V} \frac{j}{2} A \frac{j}{e} \frac{1}{M}, \quad \alpha = \frac{\tilde{\alpha}}{M}. \end{aligned} \quad (5)$$

Coefficients ω_H , ω_K , and ω_j have the dimension of frequency. The first two quantities are given by the regular expressions for frequencies associated with magnetic field and anisotropy energy. The third one is the new expression for a frequency associated with a current.

The behavior of the small piece will be completely determined by these parameters. The orientation of $\vec{\omega}_H$ and \mathbf{s} vectors with respect to the principal axis of the anisotropy tensor $\hat{\omega}_K$ is the only connection between the spin space and real space that exists in the problem. For example, the direction of the current j with respect to the anisotropy axis is irrelevant. The only thing that matters is which of the magnetic pieces is upstream and which is downstream with respect to the flow of electrons, so the current is a scalar variable. As explained above, the dependence $\mathbf{s} = \mathbf{s}(\vec{\omega}_H)$ is given by the properties of the polarizer.

The vector equation (4) has the form

$$\dot{\mathbf{n}} - \alpha [\mathbf{n} \times \dot{\mathbf{n}}] = \mathbf{F}(\mathbf{n}), \quad (6)$$

where we have moved all terms with a derivative to the right. First we transform this vector equation on $\mathbf{n}(t)$ into a system of equations on the polar angles $\phi(t)$, $\theta(t)$ which are defined in the standard way (see Appendix B for derivation). This gives

$$\begin{bmatrix} \sin \theta & -\alpha \\ -\alpha \sin \theta & -1 \end{bmatrix} \begin{Bmatrix} \dot{\phi} \\ \dot{\theta} \end{Bmatrix} = \begin{Bmatrix} v_\phi(\phi, \theta) \\ v_\theta(\phi, \theta) \end{Bmatrix}$$

or

$$\begin{Bmatrix} \dot{\phi} \\ \dot{\theta} \end{Bmatrix} = \frac{1}{1 + \alpha^2} \begin{vmatrix} 1/\sin \theta & -\alpha/\sin \theta \\ -\alpha & -1 \end{vmatrix} \begin{Bmatrix} v_\phi \\ v_\theta \end{Bmatrix}. \quad (7)$$

To find equilibrium positions one must solve

$$v_\phi = 0, \quad v_\theta = 0 \quad (8)$$

from which all equilibrium points (θ_i, ϕ_i) would be obtained. Near each equilibrium Eq. (7) can be linearized,

$$\begin{aligned} \hat{V} \equiv & \begin{vmatrix} \partial v_\phi / \partial \phi & ; & \partial v_\phi / \partial \theta \\ \partial v_\theta / \partial \phi & ; & \partial v_\theta / \partial \theta \end{vmatrix} \begin{Bmatrix} \delta \phi \\ \delta \theta \end{Bmatrix} \\ = & \frac{1}{1 + \alpha^2} \begin{vmatrix} 1/\sin \theta & -\alpha/\sin \theta \\ -\alpha & -1 \end{vmatrix} \hat{V} \begin{Bmatrix} \delta \phi \\ \delta \theta \end{Bmatrix} \\ = & \hat{D} \begin{Bmatrix} \delta \phi \\ \delta \theta \end{Bmatrix}. \end{aligned} \quad (9)$$

We will call \hat{D} a ‘‘dynamic matrix.’’ It’s eigenvalues $\mu_{1,2}$ determine the nature of the equilibrium. When the eigenval-

ues are complex conjugate $\mu_{1,2} = \text{Re}\mu \pm i\text{Im}\mu$, one has a focus, which is stable for $\text{Re}\mu < 0$ and unstable in the opposite case. For two real μ 's one has a stable center for $\mu_{1,2} < 0$, an unstable center for $0 < \mu_{1,2}$, and a saddle for $\mu_1 < 0 < \mu_2$.

Below we are going to calculate the switching diagrams for two experimental situations. The first one is simpler and easier to interpret, but requires a modification of structures used in experiment. The second one corresponds to the actual experiment of the Cornell group,¹⁰ and shows a much more complicated behavior, including the stabilization of new ‘‘canted’’ configurations which would never be stable without the current.

III. AXIAL CASE

A. Axial case switching diagram

Assume that the polarizer is characterized by an easy-axis anisotropy. The small piece has a uniaxial anisotropy with respect to the same axis, with the total anisotropy energy given by

$$-\frac{1}{2}K(\mathbf{n} \cdot \vec{\nu})^2,$$

where $\vec{\nu}$ is the direction of the axis and K can have either sign. One will have an easy axis for $K > 0$ and an easy plane for $K < 0$. Next, assume that the external magnetic field is also directed along $\vec{\nu}$. Such situation with $K > 0$ was considered before³² using a different method.

The total anisotropy of each magnetic piece is given by a sum of the magnetocrystalline anisotropy and shape anisotropy. The shape anisotropy will be an easy axis for a long cylinder ($L \gg 2R$, where R is the wire radius and an easy plane for the disk ($L \ll 2R$) with $\vec{\nu}$ along the wire. To obtain the total anisotropy with the same axis, one has to choose a material with a uniaxial anisotropy along a certain crystal axis and grow it with this axis being parallel to the wire.

For example, it was found^{46,47} that cobalt nanowires grow with intrinsic easy axis perpendicular to the wire for large wire diameters $R \geq 25$ nm (‘‘thick wire’’) and with easy axis along the wire for smaller R (‘‘thin wire’’). With a thin wire one can realize both $K > 0$ and $K < 0$ cases. For $L_S \gg 2R$ the shape and magnetocrystalline anisotropies add to an easy axis along the wire. For $L_S \ll 2R$ they subtract and the total constant is given by $K = K^{(intr)} - 4\pi M^2$. If M is sufficiently large, one has an easy plane anisotropy. For cobalt $K = 5 \times 10^6$ erg/sm³ and $M = 1.4 \times 10^3$ emu, so as L_S is decreased, there will be a transition from an easy axis to an easy plane.

We find (v_ϕ, v_θ) according to Appendix B, where for the axial case

$$\mathbf{F} = [(\vec{\omega}_H - K(\mathbf{n} \cdot \vec{\nu})\vec{\nu}) \times \mathbf{n}] + \omega_j g(P, \mathbf{sn})[\mathbf{n} \times [\mathbf{s} \times \mathbf{n}]]$$

and we are free to choose $\hat{z} = \vec{\nu}$. The calculation is straightforward and we find that the equilibrium positions are given by

$$v_\phi = \omega_H \sin \theta + \omega_K \cos \theta \sin \theta = 0, \quad (10)$$

$$v_\theta = \omega_j g(\cos \theta) \sin \theta = 0.$$

In the axial case we have a special property: g is independent of ϕ . Also, Eqs. (10) were derived with the assumption that the direction of \mathbf{s} does not depend on \mathbf{B} . In reality the polarizer will be switched by sufficiently large negative magnetic field and v_ϕ, v_θ will change. We will discuss this issue at the end of this section.

When $\omega_j \neq 0$, the system can be only satisfied if $\sin \theta = 0$, i.e., the only stable positions of \mathbf{n} on the unit sphere are the North and South Poles, independent of the current value. For $\omega_j = 0$ there is an additional set of equilibrium points: a parallel determined by $\cos \theta = -\omega_H/\omega_K$.

Our next step is to determine the stability of equilibria. Equation (9) cannot be used directly when $\sin \theta = 0$ [at $\theta = (0, \pi)$ the mapping of the spherical surface on the (ϕ, θ) plane is singular]. To study dynamics in the neighborhood of these points one has to either change the direction of \hat{z} axis or use the local nonsingular coordinates, e.g., $x = \theta \cos \phi, y = \theta \sin \phi$, near the North Pole. The latter proves to be easier. We get

$$\begin{cases} \dot{x} \\ \dot{y} \end{cases} = \begin{bmatrix} -\theta \sin \phi & \cos \phi \\ \theta \cos \phi & \sin \phi \end{bmatrix} \begin{cases} \dot{\phi} \\ \dot{\theta} \end{cases}, \quad (11)$$

substitute $(\dot{\phi}, \dot{\theta})$ from Eqs. (9) and (10), and linearize Eq. (11) in (x, y) :

$$\begin{cases} \dot{x} \\ \dot{y} \end{cases} = \frac{1}{1 + \alpha^2} \hat{D}_1 \begin{cases} x \\ y \end{cases}, \quad (12)$$

$$\hat{D}_1 = \begin{bmatrix} -[\omega_j g_n + \alpha(\omega_H + \omega_K)] & -(\omega_H + \omega_K - \alpha\omega_j g_n) \\ \omega_H + \omega_K - \alpha\omega_j g_n & -[\omega_j g_n + \alpha(\omega_H + \omega_K)] \end{bmatrix},$$

$$g_n = g(P, 1).$$

The Gilbert damping coefficient α is small and we expand it up to the first order. Then the eigenvalues of the approximate dynamic matrix are

$$\mu_N = -\omega_j g(1) - \alpha(\omega_H + \omega_K) \pm i[\omega_H + \omega_K - \alpha\omega_j g(1)]. \quad (13)$$

Several general remarks should be made. We deal with 2×2 dynamic matrices the eigenvalues of which always have the form

$$\mu_{1,2} = A(\omega_H, \omega_j) \pm \sqrt{B(\omega_H, \omega_j)}. \quad (14)$$

Two important lines in the (ω_H, ω_j) parameter space are defined by equations $A = 0$ and $B = 0$. In the $B < 0$ domain the eigenvalues are complex conjugate. Here crossing the $A = 0$ line means changing the nature of the focus between stable and unstable. In the $B > 0$ both eigenvalues are real. The $A = 0$ line is irrelevant, but two additional lines emerge: $\mu_1 = A + \sqrt{B} = 0$ and $\mu_2 = A - \sqrt{B} = 0$. They divide the $B > 0$ domain of the parameter space into three regions where the equilibrium is a stable focus, an unstable focus, and a saddle. The general situation of such a division is shown in Fig. 2.

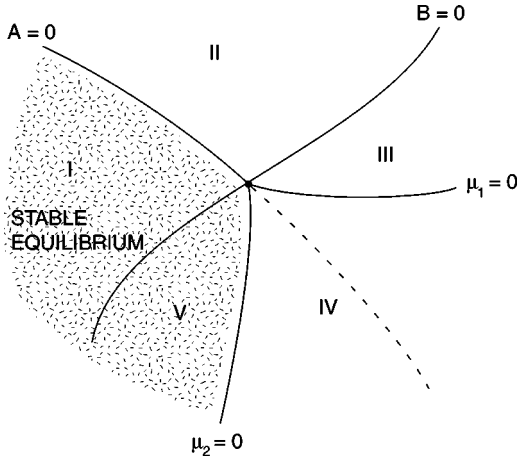


FIG. 2. Generic shape of the switching diagram near the crossing of the $A=0$ and $B=0$ lines (see text): (I) stable focus, $A < 0$, $B < 0$; (II) unstable focus, $A > 0$, $B < 0$; (III) unstable center $B > 0$, $\mu_{1,2} > 0$; (IV) saddle $B > 0$, $\mu_1 < 0 < \mu_2$; and (V) stable center $B > 0$, $\mu_{1,2} < 0$.

In the axial case the situation is degenerate: $B \leq 0$ everywhere. The North Pole is a focus [except for the line given by $\omega_H + \omega_K - \alpha \omega_j g(1) = 0$, where it is a center], which is stable for

$$\omega_{jN} > -\frac{\alpha(\omega_H + \omega_K)}{g(P, 1)}. \quad (15)$$

We see that the “critical current” needed to get to the stability boundary is proportional to the small α . This will be the case for all equilibria we consider in this paper. In that sense the switching current will be sometimes obtained by expanding the formulas in small $\omega_j \sim \alpha(\omega_K, \omega_H)$. Experimentally, however, the “small” currents are of the order 10^7 A/cm². We will comment on the other instabilities happening for large currents $\omega_j \sim \omega_K, \omega_H$, but these instabilities are not probed in the present-day experiments.

Switching happens when the equilibrium changes its nature from a stable to an unstable focus. Without the current the focus is stable due to the positiveness of the Gilbert damping coefficient α , which, in turn, is the consequence of the energy dissipation in the magnetic piece. The equilibrium becomes unstable not because the potential energy changes from a local minimum to a local maximum or a saddle, but because the total damping gets negative. The physical reason is the possibility to extract energy from the flow of current through the piece. Here it is useful to note that the spin-transfer term in Eq. (4) cannot be absorbed by a change of the energy F , i.e., it is not a gradient of any function. To prove this statement one can check that the curl of the spin-transfer term is nonzero.

For the South Pole we perform the same linearization. The nonsingular coordinates now are $x = -\delta\theta \cos \phi$, $y = -\delta\theta \sin \phi$ with $\delta\theta \equiv \theta - \pi$ and the dynamic matrix has the form

$$\hat{D} = \begin{bmatrix} -[\omega_j g_s + \alpha(\omega_H - \omega_K)] & \omega_H - \omega_K - \alpha \omega_j g_s \\ \omega_H - \omega_K - \alpha \omega_j g_s & \omega_j g_s + \alpha(\omega_H - \omega_K) \end{bmatrix},$$

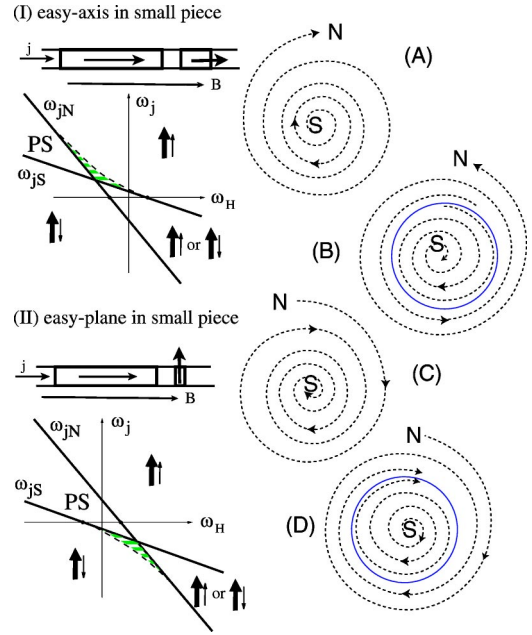


FIG. 3. (Color online) Switching phase diagram for the axial case. (I) Easy axis in the small piece; (II) easy plane in the small piece. Regions are marked either by listing possible stable configurations (thick arrow represents \mathbf{s} and thin arrow represents \mathbf{n}) or by PS which is the precession region. The small hatched regions are discussed in Sec. III B. Time-evolution flow on the projected sphere (N is mapped to infinity and S to the origin) is shown for the case of easy axis: (A) For stable North Pole, (B) for bistable region, (C) for stable South Pole, and (D) for stable precession cycle. The easy-plane flow is slightly more complicated, as explained in Appendix C.

$$g_s = g(P, -1). \quad (16)$$

The eigenvalues are

$$\mu_S = \omega_j g(-1) + \alpha(\omega_H - \omega_K) \pm i|\omega_H - \omega_K - \alpha \omega_j g(-1)| \quad (17)$$

and the stability condition is

$$\omega_{jS} < -\frac{\alpha(\omega_H - \omega_K)}{g(P, -1)}. \quad (18)$$

The regions of stability of the North and South Poles are shown in Fig. 3. In this figure we also show the flow pattern on the unit sphere. To do that we project the sphere on the plane, so that the South Pole is represented by the origin and the North Pole is projected to infinity. First of all, we see that there is a region where neither equilibrium is stable. This will be discussed in the following section. Out of the other three regions two have just one stable state and the third one has two stable states. In the former cases any initial position of \mathbf{n} on the sphere evolves into the corresponding stable equilibrium. In the latter case, the sphere is divided into two parts: the basins of attraction to both equilibria. This situation closely resembles the one with one absolute minimum and one metastable minimum of energy. However one has to remember that energy is not conserved in the presence of the current and we obtained the information about the flow and

stability of equilibria not from the energy minimization, but from the dynamic equations analysis. The phase flow diagrams for cases with one and two stable points are shown in Fig. 3(A,B,C). In Fig. 3(I,II) we show regions of stability, indicating bistable regimes which will produce hysteresis upon switching in current with fixed magnetic field, for example.

When a current is changed at fixed ω_H the system will follow a vertical line on the phase diagrams shown in Fig. 3(I,II). If this line crosses the bistable region, a hysteretic behavior will be observed. For example if one starts from the domain where only parallel configuration is stable and decreases the current, the configuration will be stable all the way down to ω_{jN} line, where a switch to the antiparallel configuration occurs. If one goes back by increasing the current, the antiparallel configuration will remain stable up to the ω_{jS} line. At both switching points a jump in the resistance of the wire will be observed due to the giant magnetoresistance effect. The case when the $\omega_H = \text{const}$ line crosses the precession region will be discussed in the following section.

B. Precession states in the axial case

It is important that there is a region on the diagram where both equilibrium points are unstable. Since the sphere is a compact manifold, this necessarily means that there exists a stable cycle, around which \mathbf{n} performs a periodic motion. Of course, the energy is still dissipated due to the presence of the Gilbert damping term in the equations. But it also can be drawn from the current. In the precession state there is a balance between the energy influx and its dissipation.

In general, stability analysis of equilibria does not give any information about the shape of such cycle. But in the axial case it is easy to guess that \mathbf{n} will be circling around a parallel determined by an angle θ_0 , such that $\dot{\theta} = 0$. From Eq. (7) this means

$$\dot{\theta} = \omega_j \frac{g(\cos \theta_0)}{\alpha} + (\omega_H + \omega_K \cos \theta_0) = 0, \quad (19)$$

$$\dot{\phi} = \omega_H + \omega_K \cos \theta_0.$$

These equations give the position of the cycle and the frequency $\omega = \dot{\phi}$ of the precession. The sign of ω gives the direction of precession. We see that ϕ does not enter Eq. (19). From the second equation $\cos \theta_0 = (\omega - \omega_H) / \omega_K$, so we reduce the system to one equation

$$\frac{\omega_j}{\alpha} g\left(\frac{\omega - \omega_H}{\omega_K}\right) + \omega = 0, \quad (20)$$

which, due to the requirement $-1 \leq \cos \theta_0 \leq 1$, should be solved on the interval

$$\omega_- \leq \omega \leq \omega_+, \quad (21)$$

$$\omega_- \equiv \omega_H - |\omega_K|, \quad \omega_+ \equiv \omega_H + |\omega_K|.$$

We rewrite $g(x)$ as

$$g(x) = \frac{1}{f(P)(3+x)-4} = \frac{1}{f(P)(x+\xi)}, \quad (22)$$

$$\xi \equiv 3 - \frac{4}{f(P)},$$

where, according to Eq. (3), $P \in [0,1]$ corresponds $f(P) \in [2, +\infty)$ and $\xi \in [1,3]$, and cast Eq. (20) in the form

$$\frac{\omega_j \omega_K}{\alpha f(P)} = -\omega(\omega - \omega_H + \xi \omega_K). \quad (23)$$

Solutions of this quadratic equation on the interval (21) are analyzed in Appendix C. First, it always has one solution in the PS region of the switching diagram. For this case the flow on the sphere is shown in Fig. 3(D). It is somewhat similar to the flow in Fig. 3(B): in both cases the upper and lower parts of the sphere are separated by a cycle, but it is a stable cycle in the former case and an unstable one in the latter case.

Second, Eq. (23) can also have solutions outside of the PS region. To understand what happens, recall that our stability analysis of the equilibrium points cannot predict the number of cycles between equilibria. It turns out, that when Eq. (23) has solutions outside the PS region, there are two cycles between South and North Poles: one stable and another unstable. An unstable cycle separates the stable cycle and the stable equilibrium. This situation will be called a ‘‘cycle-and-pole’’ state. Its domain of existence is shown in Fig. 3(I,II) by the hatched regions and is labeled as PS+N or PS+S on the switching diagram, where the second letter denotes the stable pole. The cycle-and-pole state transforms into a state with a single stable pole when stable and unstable cycles merge and annihilate. This event happens far away from the equilibrium points and therefore cannot be detected by studying their stability.

It is instructive to follow the transformation of the flow pattern as ω_j changes from large positive to large negative values at a fixed ω_H . For example, let us consider the case of $\omega_K < 0$ and choose ω_H so that during the ω_j sweep we will cross both the PS region and PS+S region (see Fig. 4). At $\omega_j = \omega_{jN}$ the North Pole becomes unstable. A stable cycle nucleates around it and starts to grow. When ω_j reaches ω_{jS} , an unstable cycle nucleates around the South Pole. This pole becomes stable and is now separated by the unstable cycle from the stable cycle. The stable and unstable cycles move towards each other, until they collide at some ω_{jc} and annihilate. After that, only the South Pole is stable.

If we would increase ω_j from a negative value, we would observe how at ω_{jc} two cycles are created on the sphere and then travel to the opposite poles. First the unstable cycle would reach the South Pole at $\omega_j = \omega_{jS}$ and disappear, then the stable cycle would reach the North Pole at $\omega_j = \omega_{jN}$ and disappear as well.

When the $\omega_H = \text{const}$ line crosses the PS region but does not cross the cycle-and-pole region, the behavior of the stable cycle is simpler. As one enters the precession region, the stable equilibrium becomes unstable by developing an infinitesimal stable cycle around itself. Upon going further

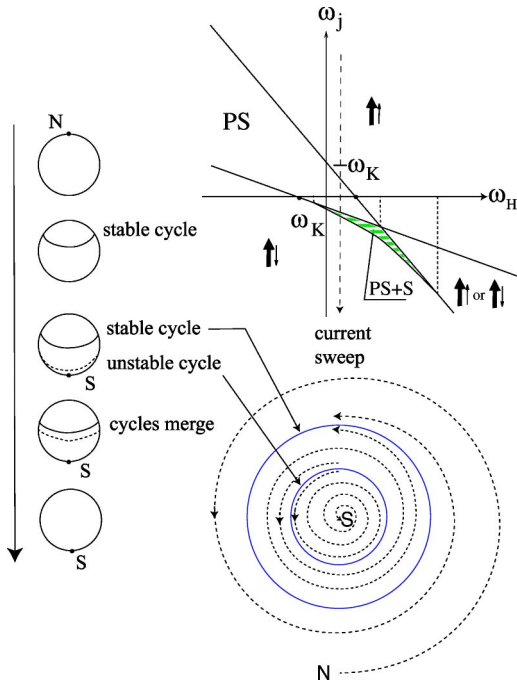


FIG. 4. (Color online) Evolution of the stable equilibria and cycles in a current sweep. The regions are marked like in Fig. 3. The value of ω_H is chosen so that both pure precession and “cycle-and-pole” (hatched) regions are crossed. Appendix C discusses the phase flow in greater detail.

into the PS region, the size of the precession cycle becomes larger and eventually the magnetization of the small piece precesses along the equator of the unit sphere. After that, the precession cycle begins to shrink around the other equilibrium. It finally converges on the other equilibrium and makes it stable. Thus as one crosses the PS region the angle of stable precession continuously changes between $\theta=0$ and $\theta=\pi$. The resistance of the wire will change continuously between the parallel and antiparallel values.

C. Evaluation of the frequency

The precession state is an interesting candidate for observation with a magnetic force microscope, which can detect the oscillations of the magnetic moment by the mechanical response of its cantilever and measure their frequency. It is shown in Appendix C that as one performs a current sweep at a fixed ω_H through the precession region two situations are possible. If at a given ω_H the cycle-and-pole state does not exist, the frequency of oscillations changes in the interval $\omega_H \pm |\omega_K|$. If the cycle-and-pole state exists, the frequency changes in the interval $[\omega_H - |\omega_K|, \omega_c]$ (see Appendix C for details). The possible value of ω_H , however, depends on the location of the precession domain on the parameter plane.

For the easy-axis case one has

$$\omega_H < -\omega_K \frac{g(-1) + g(1)}{g(-1) - g(1)} < 0$$

in the PS domain. Therefore by the order of magnitude precession has a frequency of ω_K and higher. In other words, the

current excites ferromagnetic resonance modes in the small magnetic piece.

In the easy-plane case ($\omega_K < 0$) the PS region includes the points with $\omega_j = 0$. At zero current the precession frequency is always zero (this is just a statement that any direction in the easy plane is an equilibrium). For the small current $\omega_j \rightarrow 0$, we have $\omega \rightarrow 0$ and its sign determines the direction of the precession. In this regime the term $\omega/\omega_K \rightarrow 0$ on the right-hand side of Eq. (20) can be neglected. This gives

$$\omega \approx \frac{\omega_j}{\alpha f (\omega_H / \omega_K + \xi)}. \quad (24)$$

To estimate ω_j we can approximate the magnetization M of the ferromagnet by $M = \mu_B / a^3$ where a is the lattice constant. Then

$$\omega_j = \gamma \frac{\hbar}{2} \frac{j}{e} \frac{1}{l_s} \frac{1}{M} = \frac{j}{e} \frac{a^3}{l_s}.$$

Taking $a = 0.5$ nm, $l_s = 10$ nm we estimate

$$\omega_j (1/s) \approx 780 j (\text{A/cm}^2).$$

Let us further assume $\alpha = 0.05$ and $P = 0.5$, so that $f = 2.4$, $\xi = 1.3$. Then

$$\left[\frac{1}{s} \right] \approx \frac{6.5 \times 10^3}{\omega_H / \omega_K + 1.3} j \left[\frac{\text{A}}{\text{cm}^2} \right].$$

In the small current approximation ($|\omega_j| \ll |\omega_K|$) used to obtain this formula it is appropriate to consider that $\omega_H / \omega_K \in [-1, 1]$ in the precession region.

D. Polarizer switch by external magnetic field

Everywhere above we implicitly assumed that the polarizer does not change its direction regardless of the magnitude of the external magnetic field. In real life this is of course not true. Even if the polarizer is made from a very hard magnetic material, large enough negative magnetic field will switch it into the opposite direction. How will that change the switching diagrams considered above?

First of all, the diagrams must be now cut off at some negative field ω_{HP} corresponding to the coercive force of the polarizer. As drawn, they are valid only for $\omega_H > \omega_{HP}$. Second, from the symmetry of the Eq. (4) it is intuitively clear (and can be derived mathematically), that with the polarizer switched to the opposite direction we can use the results for the point $(\omega_j, -\omega_H)$ on the already available switching diagram. The corresponding equilibrium directions of the analyzer will be the same relative to the new direction of \mathbf{s} . The new switching diagram will be a mirror reflected image of the original one. Note that this symmetry argument is only valid when vectors \mathbf{s} and \mathbf{B} lie in one of three planes formed by principal axes of the anisotropy tensor $\hat{\omega}_K$, which is true in all cases discussed in the present paper.

If during the experiment some polarizer switching events occur, both switching diagrams, for the original direction of the polarizer and for the reversed direction, have to be used.

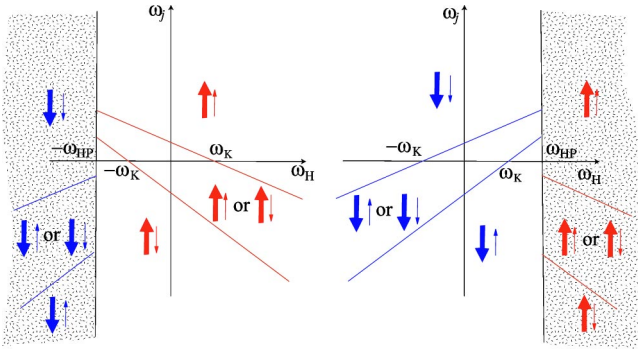


FIG. 5. (Color online) Switching diagrams for the easy-axis case with the polarizer switching at the coercive field $\pm \omega_{HP}$. It is assumed that $|\omega_{HP}|$ is less than the field of precession state onset. The left panel shows the diagram for \mathbf{s} prepared pointing along the $+z$ direction. At $\omega_H = -\omega_{HP}$ a polarizer switch to the $-z$ direction occurs after which the right panel is applicable. The polarizer switches back if the field is increased up to $+\omega_{HP}$. Then the left panel becomes again applicable.

An example of this is shown in Fig. 5 for the axial case with analyzer having easy-axis anisotropy.

IV. AXIS AND PLANE CASE

Here we expand the treatment for the case when all three principal components of $\hat{\omega}_K$ are different. In particular we will assume that the small piece has two contributions to anisotropy: an easy plane and an easy axis that is directed in this plane. This is the actual anisotropy pattern of the Cornell group experiment¹⁰ (see Fig. 6). Magnetic pieces there are thin disks—that give an easy-plane contribution to $\hat{\omega}_K$ (the plane is the plane of the disk, i.e., in this experiment it is perpendicular to the wire). The easy-axis contribution comes from either magnetocrystalline anisotropy that has an axis perpendicular to the wire, or from the additional shape contribution in the case of the noncylindrical nanopillar studied in Ref. 11. In accord with the experimental setting we as-

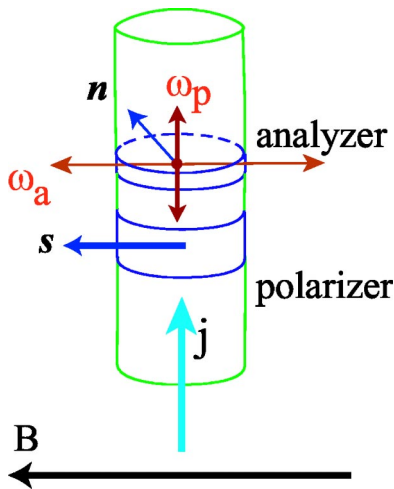


FIG. 6. (Color online) Schematic view of the Cornell group “nanopillar” and its anisotropies.

sume that a specific direction of the external magnetic field, namely, \mathbf{B} , is collinear with the easy axis of the pieces. In the paper of Sun³¹ this arrangement is called an “on-axis” geometry. We will denote the strength of the easy-plane anisotropy by $\omega_p \geq 0$ and the easy-axis anisotropy by $\omega_a \geq 0$.

We note that in the actual experiment¹⁰ the polarizer was designed to switch in a very low magnetic field.⁴⁸ Therefore only the $\omega_H > 0$ part of the switching diagram is probed (see Sec. III D). However we present results for arbitrary ω_H which can be useful for the future setups.

The “axis and plane” anisotropy has both cases considered in Sec. III as its limiting cases. If we set $\omega_p = 0$, equations will reduce to those of the “axial easy axis” case for $\omega_a > 0$ and to those of the “axial easy plane” for $\omega_a < 0$. Here we want to remind that spin transfer is independent of the relative orientation of the current \mathbf{j} and spin polarization \mathbf{s} (see Sec. II). What matters is the relative orientation of \mathbf{s} with respect to the principal axis of \hat{K} . If one could prepare a sample with pure easy axis perpendicular to the wire and put it in the external field along this axis, the system would behave in the same way as the axial easy axis of Sec. III.

To study the axis and plane case we will use two coordinate systems, characterized by different z axis of the spherical coordinates in the spin space. In the z_{\perp} system, the z axis is perpendicular to the easy-plane, and in the z_{\parallel} system it is aligned along the easy axis (and \mathbf{s}). We do that to avoid working with equilibria near the North and South Poles, which are the singular points of the polar coordinate system. As we saw in Sec. III, one has to modify coordinates to study the stability of an equilibrium point if it happens to coincide with N or S. We will see that in the axis and plane case there are four equilibrium directions of \mathbf{n} : two collinear directions $\mathbf{n} \uparrow \uparrow \mathbf{s}$, $\mathbf{n} \uparrow \downarrow \mathbf{s}$ and two canted directions \mathbf{n}_C and \mathbf{n}_D . If only one spin coordinate system is used, some of these directions under certain conditions approach N and S. By using two coordinate systems one can avoid the difficulties in studying the stability of those equilibria.

A. Calculation in the z_{\perp} system: Collinear equilibria

The magnetic field is given by $\vec{\omega}_H = \omega_H \mathbf{e}_x$, the polarizer direction by $\mathbf{s} = \mathbf{e}_x$, and the anisotropy tensor by

$$\hat{\omega}_K = \begin{vmatrix} \omega_a & 0 & 0 \\ 0 & 0 & 0 \\ 0 & 0 & -\omega_p \end{vmatrix}.$$

We now substitute that into Eq. (4) and following Appendix B we derive

$$v_{\phi} = -h \cos \theta \cos \phi - (K_p + K_a \cos^2 \phi) \sin \theta \cos \theta - Ig \sin \phi,$$

$$v_{\theta} = h \sin \phi + K_a \sin \theta \sin \phi \cos \phi - Ig \cos \theta \cos \phi, \quad (25)$$

$$g = g(\sin \theta \cos \phi, P).$$

1. Equilibrium directions of \mathbf{n}

First we observe, that Eqs. (25) can be rewritten in the form

$$v_\phi = \cos \theta [-h \cos \phi - (K_p + K_a \cos^2 \phi) \sin \theta] - Ig \sin \phi,$$

$$v_\theta = \sin \phi (h + K_a \sin \theta \cos \phi) - Ig \cos \theta \cos \phi,$$

which clearly shows that there is a solution $\cos \theta = 0$, $\sin \phi = 0$. This defines two equilibrium directions of \mathbf{n} : parallel (\mathbf{n}_A : $\theta = \pi/2$, $\phi = 0$) and antiparallel (\mathbf{n}_B : $\theta = \pi/2$, $\phi = \pi$) to \mathbf{s} . Positions of these equilibria do not depend on the current and applied magnetic field. In the z_\perp coordinates we will be studying only those two equilibria. Other equilibria will be studied in the z_\parallel coordinates.

2. Stability analysis of the collinear equilibria

For an arbitrary point (ϕ, θ) one has the expansion

$$\begin{pmatrix} \delta v_\phi \\ \delta v_\theta \end{pmatrix} = \begin{vmatrix} V_{11} & V_{12} \\ V_{21} & V_{22} \end{vmatrix} \begin{pmatrix} \delta \phi \\ \delta \theta \end{pmatrix}, \quad (26)$$

$$V_{11} = \omega_H \cos \theta \sin \phi + 2\omega_a \sin \theta \cos \theta \sin \phi \cos \phi - \omega_j g \cos \phi - \omega_j f g^2 \sin \theta \sin^2 \phi,$$

$$V_{12} = \omega_H \sin \theta \cos \phi + (\sin^2 \theta - \cos^2 \theta)(\omega_a \cos^2 \phi + \omega_p) + \omega_j f g^2 \cos \theta \sin \phi \cos \phi,$$

$$V_{21} = \omega_H \cos \phi + \omega_a \sin \theta (\cos^2 \phi - \sin^2 \phi) + \omega_j g \cos \theta \sin \phi (1 - fg \sin \theta \cos \phi),$$

$$V_{22} = \omega_a \cos \theta \sin \phi \cos \phi + \omega_j g \cos \phi (\sin \theta + fg \cos^2 \theta \cos \phi).$$

Now for the equilibrium direction \mathbf{n}_A we obtain

$$\hat{V}_A = \begin{vmatrix} -\omega_j g(1, P) & \omega_H + (\omega_a + \omega_p) \\ \omega_H + \omega_a & \omega_j g(1, P) \end{vmatrix}.$$

The dynamic matrix for $\sin \theta = 1$ is given by

$$D_A = \begin{vmatrix} 1 & -\alpha \\ -\alpha & -1 \end{vmatrix} \hat{V} = \begin{vmatrix} -\omega_j g_A - \alpha(\omega_H + \omega_a) & \omega_H + \omega_a + \omega_p \\ -(\omega_H + \omega_a) & -I g_A - \alpha(\omega_H + \omega_a + \omega_p) \end{vmatrix},$$

where $g_A = g(1, P)$, and has the following eigenvalues:

$$\mu_A = -[\omega_j g_A + \alpha(\omega_H + \omega_a + \omega_p/2)] \pm \sqrt{-(\omega_H + \omega_a)(\omega_H + \omega_a + \omega_p)}.$$

Here we calculated up to the lowest order in α . We see that in terms of the discussion of Eq. (14) the expression for $B(\omega_H, \omega_j)$ contains zero order terms, i.e., small current cannot change its sign and we may neglect the higher terms. However $A(\omega_H, \omega_j)$ starts with terms linear in α and ω_j .

Therefore small current can switch between stable and unstable foci. In the present case $B(\omega_H, \omega_j)$ is positive for $-(\omega_a + \omega_p) \leq \omega_H \leq -\omega_a$ and negative otherwise. We may conclude that everywhere inside the interval $[-(\omega_a + \omega_p), -\omega_a]$, except very close to its ends where the square root term and the first term are comparable, the eigenvalues μ_A are real numbers with opposite signs and so the equilibrium is a saddle. In terms of Fig. 2 regions III and V become very narrow wedges and we ignore them in our discussion. Outside of the interval $[-(\omega_a + \omega_p), -\omega_a]$ the equilibrium is a focus, stability of which (again everywhere except very close to the ends of the interval where higher-order terms in the α expansion will play a role) is determined by $\text{Re} \mu_A < 0$. We get two conditions for the stability region of the \mathbf{n}_A equilibrium:

$$\omega_j \geq -\alpha \frac{2\omega_H + 2\omega_a + \omega_p}{2g(1, P)}, \quad (27)$$

$$\omega_H \leq -(\omega_a + \omega_p) \quad \text{or} \quad \omega_H \geq -\omega_a.$$

For the antiparallel equilibrium \mathbf{n}_B we have

$$\hat{V}_B = \begin{vmatrix} \omega_j g(-1, P) & -\omega_H + (\omega_a + \omega_p) \\ -\omega_H + \omega_a & -\omega_j g(-1, P) \end{vmatrix}$$

and the dynamic matrix

$$D_B = \begin{vmatrix} 1 & -\alpha \\ -\alpha & -1 \end{vmatrix} \hat{V}_B = \begin{vmatrix} \omega_j g_B - \alpha(-\omega_H + \omega_a) & -\omega_H + \omega_a + \omega_p \\ \omega_H - \omega_a & \omega_j g_B \alpha(-\omega_H + \omega_a + \omega_p) \end{vmatrix}$$

with $g_B = g(-1, P)$. The eigenvalues are

$$\mu_B = \omega_j g_B - \alpha(-\omega_H + \omega_a + \omega_p/2) \pm \sqrt{-(\omega_a - \omega_H)(\omega_a + \omega_p - \omega_H)}.$$

Now $B(\omega_H, \omega_j)$ is positive for $\omega_a \leq \omega_H \leq \omega_a + \omega_p$ and negative otherwise, and the conclusion, valid again everywhere except very close to the ends of this interval, is that inside the interval the point is a saddle and outside it is a focus. The stability of the focus is given by $\text{Re} \mu_B < 0$. Together with the domain of existence of the focus it gives two conditions

$$\omega_j \leq \alpha \frac{-2\omega_H + 2\omega_a + \omega_p}{2g(-1, P)},$$

$$\omega_H \geq \omega_a + \omega_p \quad \text{or} \quad \omega_H \leq \omega_a.$$

B. Calculation in the z_\parallel system: Noncollinear equilibria

First we repeat the derivation of v_ϕ, v_θ . The magnetic field is equal to $\vec{\omega}_H = \omega_H \mathbf{e}_z$, the polarizer direction is given by $\mathbf{s} = \mathbf{e}_z$ and the anisotropy tensor is equal to

$$\hat{\omega}_K = \begin{vmatrix} -\omega_p & 0 & 0 \\ 0 & 0 & 0 \\ 0 & 0 & \omega_a \end{vmatrix}.$$

Again with Eq. (4) and Appendix B we derive

$$\begin{aligned} v_\phi &= h \sin \theta - (K_a + K_p \cos^2 \phi) \sin \theta \cos \theta, \\ v_\theta &= -K_p \sin \theta \sin \phi \cos \phi + I g \sin \theta, \\ g &= g(\cos \theta, P). \end{aligned} \quad (28)$$

We see that the $z_{||}$ coordinate system gives simpler expressions for the force projections v_ϕ, v_θ , and recall that the only reason for doing the calculation in the z_\perp coordinates was to avoid the singularities associated with the equilibrium directions $\mathbf{n}_{A/B}$ in the $z_{||}$ system.

1. Equilibrium directions

First of all we see that $\sin \theta = 0$ solves Eqs. (28). This corresponds to points $\theta = 0$ and $\theta = \pi$ i.e., directions \mathbf{n}_A and \mathbf{n}_B that were already considered before. For $\sin \theta \neq 0$ we have the following system:

$$\begin{aligned} \omega_H - (\omega_a + \omega_p \cos^2 \phi) \cos \theta &= 0, \\ \omega_p \sin \phi \cos \phi + \omega_j g &= 0, \end{aligned}$$

from where we get

$$\begin{aligned} \cos \theta &= -\frac{\omega_H}{\omega_a + \omega_p \cos^2 \phi}, \\ \omega_p \sin \phi \cos \phi &= \omega_j g(\cos \theta, P). \end{aligned}$$

From the first equation we can get expressions for $\cos^2 \phi$ and $\sin^2 \phi$ through $\cos \theta$ as

$$\begin{aligned} \cos^2 \phi &= \frac{-\omega_a - \omega_H / \cos \theta}{\omega_p}, \\ \sin^2 \phi &= \frac{\omega_p + \omega_a + \omega_H / \cos \theta}{\omega_p}. \end{aligned} \quad (29)$$

We substitute these expressions into the second equation squared, use the form of g , Eq. (22), and get

$$-[(\omega_p + \omega_a) \cos \theta + \omega_H](\omega_a \cos \theta + \omega_H) = \frac{\omega_j^2 \cos^2 \theta}{f^2 (\cos \theta + \xi)^2}. \quad (30)$$

The plots of both sides as a function of $z = \cos \theta$ are shown in Fig. 7. There are two solutions: points C and D . These are states whose magnetization lies at an angle, canted, to the easy axis (and \mathbf{s} and \mathbf{B}). For zero current we get

$$\begin{aligned} \cos \theta_C &= -\omega_H / (\omega_a + \omega_p), \quad \sin \phi_C = 0, \\ \cos \theta_D &= -\omega_H / \omega_a, \quad \cos \phi_D = 0. \end{aligned} \quad (31)$$

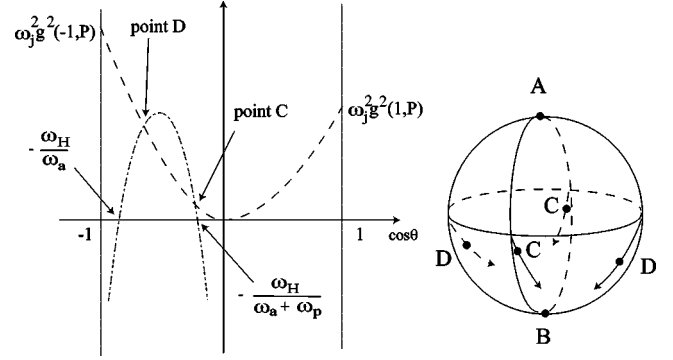


FIG. 7. Left panel: graphical solution of Eq. (30) for the $\omega_H > 0$ case. The left-hand side of Eq. (30) is represented by a dashed-dotted line and the right-hand side is represented by a dashed line. Right panel: The trajectories of the points C and D on the sphere as their position changes with increasing current.

Dependence of the solutions of Eq. (30) on the parameters ω_H and ω_j means that by changing these parameters one can change the equilibrium directions $\mathbf{n}_{C/D}$, or equivalently move points C and D along the surface of the unit sphere as sketched in Fig. 7. From the graphic solution we can conclude qualitatively that when current is increased at fixed magnetic field, C and D move towards each other, eventually merge, and annihilate. When magnetic field is changed at fixed current, C and D move towards North or South Poles of the z_\perp coordinate system, and merge with $\mathbf{n}_{A/B}$ equilibria.

We start by looking for the domains of existence of the solutions C and D . Since Eq. (30) is a fourth-order algebraic equation, it has to be solved numerically. A representative picture is shown in Fig. 8. The characteristic height of the domes in this picture can be estimated at $\omega_H = 0$,

$$\omega_{j \max} \approx f \xi \sqrt{(\omega_a + \omega_p) \omega_a}. \quad (32)$$

2. Stability analysis of \mathbf{n}_B and \mathbf{n}_C equilibria

First of all one can check that at zero current C and D equilibria correspond to the maxima of the magnetic energy. They are therefore unstable and play no role in the usual magnetic studies. However we will see below that in the presence of the current they can be stabilized. In a sense this is a phenomenon opposite to the one discussed in Sec. III A. There a stable equilibrium was destabilized by the current.

Expansion of v_ϕ, v_θ gives the \hat{V} matrix defined in Eq. (9),

$$\hat{V} = \begin{vmatrix} -\frac{\omega_p}{2} \sin 2\phi \cos 2\theta & U \\ -\omega_p \sin \theta \cos 2\phi & -\frac{\omega_p}{2} \cos \theta \sin 2\phi + \omega_j g W \end{vmatrix},$$

$$W = (\cos \theta + f g \sin^2 \theta),$$

$$U = \omega_H \cos \theta + \cos 2\theta (\omega_a + \omega_p \cos^2 \phi),$$

where we used $\delta g = f g^2 \sin \theta \delta \theta$ in the $z_{||}$ system. The dynamic matrix

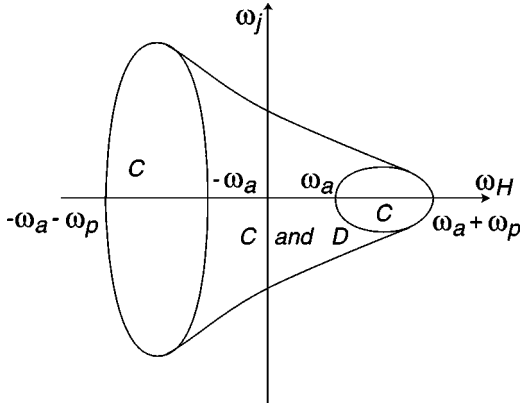


FIG. 8. Domains of existence of solutions C and D for $\omega_a = \omega_p$. For zero current D exists for $-\omega_a \leq \omega_H \leq \omega_a$ and C exists for $-\omega_a - \omega_p \leq \omega_H \leq \omega_a + \omega_p$. However for finite current D can exist for a larger interval.

$$\hat{D} = \begin{vmatrix} 1/\sin \theta & -\alpha/\sin \theta \\ -\alpha & -1 \end{vmatrix} \quad \hat{V} = \begin{vmatrix} D_{11} & D_{12} \\ D_{21} & D_{22} \end{vmatrix}$$

has components

$$D_{11} = \omega_p(-\cos \theta \sin 2\phi + \alpha \cos 2\phi),$$

$$D_{12} = U/\sin \theta + \frac{\alpha \omega_p \cos \theta \sin 2\phi}{2 \sin \theta} - \frac{\alpha \omega_j g W}{\sin \theta},$$

$$D_{21} = \omega_p(\sin \theta \cos 2\phi + \frac{1}{2} \sin 2\phi \sin 2\theta),$$

$$D_{22} = -\alpha U + \frac{\omega_p}{2} \cos \theta \sin 2\phi + \omega_j g W,$$

and the eigenvalues are given by

$$\mu = \frac{D_{11} + D_{22}}{2} \pm \sqrt{\frac{(D_{11} - D_{22})^2}{2} + D_{12}D_{21}}. \quad (33)$$

At the equilibrium directions using Eqs. (28) and (29) we have

$$\sin 2\phi = \frac{2\omega_j g}{\omega_p},$$

$$\cos 2\phi = -\frac{2\omega_a + \omega_p + 2\omega_H/\cos \theta}{\omega_p},$$

$$\cos^2 \phi = \frac{-\omega_a - \omega_H/\cos \theta}{\omega_p},$$

which makes it possible to express all ϕ -dependent terms in \hat{D} through $\cos \theta$. This gives $U = \omega_H(1 - \cos^2 \theta)/\cos \theta$ and then

$$D_{11} = -2\omega_j g \cos \theta \alpha \left(2\omega_a + \omega_p + \frac{2\omega_H}{\cos \theta} \right),$$

$$D_{12} = \frac{1}{\sin \theta} \left(\omega_H \frac{1 - \cos^2 \theta}{\cos \theta} + \alpha \omega_j g (\cos \theta - W) \right),$$

$$D_{21} = \sin \theta \left(2\alpha \omega_j g \cos \theta - 2\omega_a - \omega_p - \frac{2\omega_H}{\cos \theta} \right), \quad (34)$$

$$D_{22} = -\alpha \omega_H \frac{1 - \cos^2 \theta}{\cos \theta} + \omega_j g (\cos \theta - W).$$

Now we can substitute Eq. (34) into Eq. (33), and get an expression $\mu(\cos \theta, \omega_j, \omega_H)$. To study stability, Eq. (30) has to be solved for $\cos \theta$ and its solution substituted into $\mu(\cos \theta, \omega_j, \omega_H)$. Knowing $\mu(\omega_j, \omega_H)$ we can divide the parameter plane (ω_j, ω_H) into regions where $\mathbf{n}_{C/D}$ exist and subregions where they are stable. For arbitrary (ω_j, ω_H) this procedure requires a numeric solution of the fourth-order algebraic equation (30).

3. Stability analysis of $\mathbf{n}_{C/D}$ equilibrium direction for small currents

Several simplifications happen when the current magnitude is small, i.e., $\omega_j \ll \omega_{j\max}$. Using Eq. (33) we see that the first term in μ , Eq. (33), is of the first order in current ω_j and damping coefficient α , while the expression under the square root starts with a zero-order term. Such situation was already discussed in Secs. III A and IV A 2: the switching between stable and unstable focuses is controlled by the first-order terms and therefore can happen for $\omega_j \sim \alpha \omega_{j\max}$.

For nonzero current points C and D move from their original positions. But from Eq. (30) we see that corrections to $\cos \theta$ are starting with the terms quadratic in ω_j , so in the linear approximation we can use Eq. (31).

To begin with, we determine whether equilibria are foci or saddles/centers. We calculate $Q = (D_{11} - D_{22})^2/4 + D_{12}D_{21}$ leaving only zero-order terms. For point C

$$Q|_C = -\left(1 - \frac{\omega_H^2}{(\omega_a + \omega_p)^2} \right) (\omega_a + \omega_p) \omega_p < 0,$$

where the last inequality is true for all values of ω_H at which C exists. Therefore C is a focus. For point D

$$Q|_D = \left(1 - \frac{\omega_H^2}{\omega_a^2} \right) \omega_a \omega_p > 0,$$

where again the inequality is always fulfilled as long as equilibrium D exists for $\omega_j \rightarrow 0$. Since $D_{11} + D_{22} \sim \alpha \omega_j$ is a small value, the eigenvalues of the dynamic matrix at point D almost always (see corresponding discussion in Sec. IV A 2) have opposite signs and hence point D is a saddle. Accordingly it is never a stable equilibrium and we can disregard it in the further analysis.

Point C is a focus, stability of which is determined by the sign of $\text{Re} \mu_C = (1/2)(D_{11} + D_{22})|_C$. Expansion of this quantity up to the linear terms in ω_j and α reads

$$\text{Re} \mu_C = \frac{1}{2} \left\{ -\omega_j g \left[\frac{-2\omega_H}{\omega_a + \omega_p} + f g \left(1 - \frac{\omega_H^2}{(\omega_a + \omega_p)^2} \right) \right] + \alpha \left(2\omega_p + \omega_a - \frac{\omega_H^2}{\omega_a + \omega_p} \right) \right\}$$

and changes sign at

$$\omega_{jC} = \frac{\alpha[2\omega_p + \omega_a - \omega_H^2/(\omega_a + \omega_p)]}{gV}, \quad (35)$$

$$V = -\frac{2\omega_H}{\omega_a + \omega_p} + fg \left(1 - \frac{\omega_H^2}{(\omega_a + \omega_p)^2} \right).$$

The numerator of the formula is positive, g is always positive as well, but V changes sign on the interval $\omega_H \in [-\omega_a - \omega_p, \omega_a + \omega_p]$ since $V(\omega_H = -\omega_a - \omega_p) = 2$ and $V(\omega_H = \omega_a + \omega_p) = -2$. We find that the point ω_* where $V = 0$ is given by

$$\omega_* = (\omega_a + \omega_p) [\xi - \sqrt{\xi^2 - 1}]$$

so that

$$(3 - 2\sqrt{2})(\omega_a + \omega_p) < \omega_* < (\omega_a + \omega_p).$$

Finally, examining the sign of $\text{Re}\mu_C$ one can check that for $\omega_H < \omega_*$ point C is stable for $\omega_j > \omega_{jC}$, and for $\omega_H < \omega_*$ it is stable for $\omega_j < \omega_{jC}$. Thus we identify a novel equilibrium phase, the canted phase. Its angle with regard to the easy axis is given to first order by Eq. (31). An example of the time-evolution flow for the case when C is stabilized by the current is shown in Fig. 9.

The stability regions of equilibria A , B , and C on the parameter plane are shown in Fig. 10. Their boundaries are given by Eqs. (27), (28), and (35). As in the axial case, there are regions where neither equilibrium is stable and thus a precession state occurs. Here we cannot make a stronger statement about the absence of the precession states in other parts of the switching diagram. In fact our experience from the axial case, where precession states were analyzed in detail, shows that such situation may well occur. This figure presents the low current limit of the switching diagram of the Cornell nanopillar device. Below we make several remarks about it.

Different types of behavior are now predicted for the experiments in which a current is swept at fixed ω_H . As mentioned at the beginning of Sec. IV, the actual experiment measures only the $\omega_H > 0$ part of the switching diagram. There are three regimes for positive magnetic field.

For $0 < \omega_H < \omega_a$ the switching pattern will be similar to the axial case, but in addition, here the canted equilibrium C will become stable for large enough positive ω_j . Since this will happen on top of already stable equilibrium A , a switch to C is unlikely. However one can put the system into the C state by following a different path on the parameter plane. To obtain the canted state at zero magnetic field, for example, one could start at negative field, increase the current past the critical value for C equilibrium, and then decrease the field to zero.

For $\omega_a < \omega_H < \omega_a + \omega_p$ the switching will happen either between A and precession state (without hysteresis) or between A and C (with hysteresis). It is important to note that

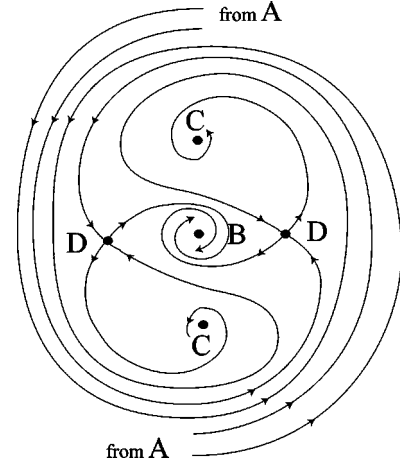


FIG. 9. Time-evolution flow when B and C are stable equilibria and A is an unstable equilibrium.

in this regime switching with hysteresis happens not between parallel and antiparallel states, but between parallel and canted states.

For $\omega_a + \omega_p < \omega_H$ we return back to hysteretic switching between A and B similar to the axial case. The canted state is never stabilized in this regime.

The experimental results⁹⁻¹² are consistent with those predictions for $0 < \omega_H < \omega_a$, where hysteretic switching was observed. They also observe several different precession regimes for $\omega_a + \omega_p < \omega_H$. The interval $\omega_a + \omega_p < \omega_H$ was not yet investigated systematically.

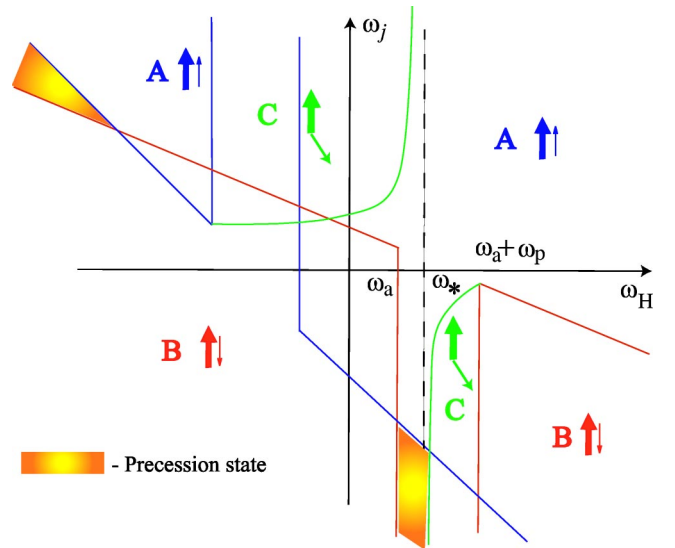


FIG. 10. (Color online) Switching diagram of the “axis and plane” case for small currents. The domains of stability are marked by letters (see text) and arrows, showing the relative orientation of \mathbf{s} (thick arrow) and \mathbf{n} (thin arrow). The parallel configuration \mathbf{n}_A is stable inside two wedges opening up, the antiparallel configuration \mathbf{n}_B is stable inside two wedges opening down, and the canted configuration \mathbf{n}_C is stable in two domains above and below the horizontal axis, but both lying inside the $\pm(\omega_a + \omega_p)$ interval. Within the shaded regions neither equilibrium is stable, thus a stable precession is happening.

C. Comments on the “axis and plane” case

It is easy to check that for $\omega_p=0$ we recover the axial case, Sec. III, Fig. 3. The only subtlety here will be that since for $\omega_p=0$ positions of the points C and D are given by the same expression $\cos \theta = \omega_H/\omega_a$, those points formally coincide. In reality those points just do not exist as we saw in Sec. III. The gap between ω_a and $\omega_a + \omega_p$ in the lines of stability of equilibria $\mathbf{n}_{A/B}$ closes for $\omega_p=0$ and thus the axial case is exactly reproduced.

Now consider the ratio of the critical currents ω_{jC} and ω_{jB} at $\omega_H=0$. One has

$$\omega_{jC}(\omega_H=0) = \alpha \frac{2\omega_p + \omega_a}{fg^2(0)} = \alpha(2\omega_p + \omega_a)f\xi^2, \quad (36)$$

$$\omega_{jB}(\omega_H=0) = \alpha \frac{2\omega_a + \omega_p}{2g(-1)} = \alpha \left(\omega_a + \frac{1}{2}\omega_p \right) f(\xi - 1).$$

Thus

$$\frac{\omega_{jC}}{\omega_{jB}} = 2 \frac{2\omega_p + \omega_a}{\omega_p + 2\omega_a} \frac{\xi^2}{\xi - 1} \geq 4$$

and the stability line of C in Fig. 10 is always higher than the stability line of B at $\omega_H \geq 0$. This is important for the comparison with the results of the Cornell group experiments,¹⁰ because there only the $\omega_H \geq 0$ region of the switching diagram is probed as explained in the beginning of Sec. IV.

When ω_H is in the vicinity of ω_* , the critical current, given by Eq. (35), diverges, violating the underlying assumption of small current. This poses a question of the real behavior of the stability boundary of C in this region. Using exact formulas from the preceding section we have performed a numeric calculation for a representative set of parameters and found that the switching boundary indeed extends upward, where it joins the line of C - D convergence as shown in Fig. 12. Recall here that the positions of points C and D are given by Eq. (31) only for small current. For larger currents Eqs. (29) and (30) must be solved. As a result the positions of C and D move along the sphere as current is increased and eventually these two points coalesce and disappear.

The canting angle depends on the current and magnetic field, and these can be used to engineer a desired “switching angle” between points C and A . This angle can be changed between 0° and 180° by sweeping the magnetic field \mathbf{B} , Eq. (31). But according to Eqs. (29) and (30) it also can be adjusted by increasing the current. To give an example, we calculated the current dependent changes $\delta\theta(j)$ and $\delta\phi(j)$ of the polar angles of point C . The magnetic field was set to $\omega_H = (\omega_a + \omega_p)/2$, which gives a $\theta_C = 120^\circ$ angle between A and C at zero current. The spin-polarization degree was taken to be $P = 35\%$, and Gilbert damping was set to $\alpha = 0.01$. In Fig. 11 $\delta\theta(j)$ and $\delta\phi(j)$ are shown as functions of j/j_C , where j_C is the minimal current stabilizing the canted state (36). Note that $\delta\theta(j)$ is much smaller than $\delta\phi(j)$. For $\omega_H = 0$ the angle θ does not change at all and point C moves along the parallel $\theta_C = 90^\circ$. Since the resistance of the structure is a function of θ_C , it would not be a very sensitive

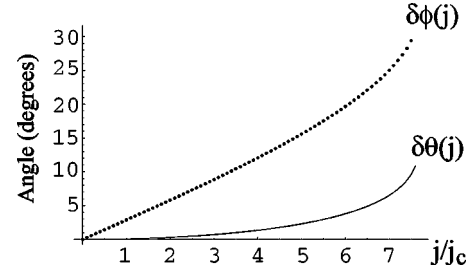


FIG. 11. Deflection of point C by a large current.

indicator of the current-induced displacements of equilibrium C . For the particular set of parameters used to plot Fig. 11 the polar angle changes are small for $j \approx j_C$. They become significant for currents $j \approx 10j_C$. These current values correspond to the upper boundary of the stable canted state in Fig. 12.

For the particular set of parameters chosen to calculate the switching diagram in Fig. 12 point C was still a focus for all the values of current, even though the argument of Sec. IV B 3 does not apply any more when the current is not small. Point D was a saddle for all currents as well. These statements were only violated very close to the merging point where $Q \rightarrow 0$ and the higher-order terms in α started to play a role (cf. Sec. IV A 2). Representative results for the switching diagram are shown in Fig. 12. We show this figure to give a general idea of the topology of the diagram for large ω_j . The actual calculations should be made as explained at the end of Sec. IV B 2, but they will be only

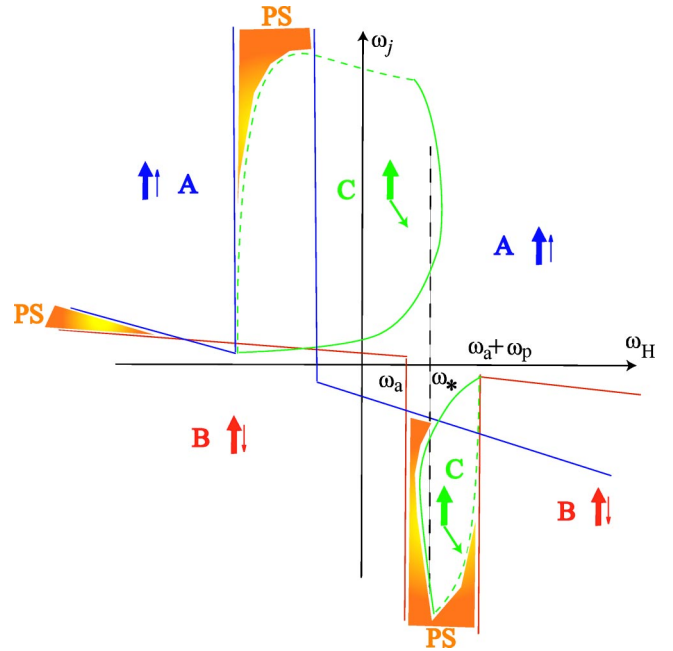


FIG. 12. (Color online) A representative switching diagram for the “axis and plane” case for all values of current. Labeling is the same as in Fig. 10. The upper boundary of the canted state stability region is the line where equilibria C and D merge. More precession regions, marked PS, show up for large currents. Figure 10 is the blowup of this figure at small currents.

needed if experimental currents could be increased by a factor of $1/\alpha \sim 100$ compared to the values of Ref. 10.

There is a restriction on P which should hold in order for us to be able to calculate in the small current approximation. Critical currents for equilibrium directions $\mathbf{n}_{A,B,C}$ are given by formulas (27), (28), and (35), each of which has α in the numerator and g , evaluated at the appropriate equilibrium point, in the denominator. In order for the small current approximation to hold the critical current must be much smaller than the current at which C and D merge, i.e., $\omega_j \ll \omega_a + \omega_b$ must be true. From here it follows that $\alpha/g \ll 1$ should hold, and since $g(x) = 1/[f(x + \xi)]$, this gives a requirement

$$\alpha f(P) \ll 1. \quad (37)$$

Here α is a small parameter, but $f(P) = (1 + P)^3 / (4P^{3/2})$ can become large as $P \rightarrow 0$. At small P we can approximate (37) by

$$P \gg (2\alpha)^{(2/3)}. \quad (38)$$

For $\alpha = 0.01$ it gives $P \gg 0.07$ which can be satisfied for materials with large spin polarization. However already for $\alpha = 0.05$ one would require $P \gg 0.22$ so the small current approximation would not be too good and one should numerically solve Eq. (30) and find the eigenvalues of the dynamic matrix given by Eq. (34).

V. CONCLUSIONS

We have obtained exact results about the stable equilibria of the magnetic piece with a spin-polarized current flowing through it. It is seen that the switching pattern depends crucially on the magnetic anisotropy and the direction of polarization of incoming current. For more complicated anisotropy new hysteresis patterns are possible and new equilibrium configurations can be stabilized. Therefore one should be careful in applying the intuition gained from a study of one anisotropy pattern to “similar” patterns. Predictions made for the axial and axis and plane cases can be used to experimentally test the spin-transfer theory,²⁶ in particular the accuracy of the factor $g(P, \mathbf{sn})$. This is especially interesting because alternative descriptions of current driven excitations are put forth in the literature. Obtained switching diagrams show that axial easy axis configuration (Fig. 3) and axis and plane configuration for the magnetic field such that ω_H lies outside of the $[\omega_a, \omega_a + \omega_p]$ interval (Fig. 10) satisfy the criteria for application in memory cells discussed in the Introduction. For other configurations and values of magnetic field the modified Landau-Lifshitz equation predicts new phenomena: stabilization of canted state and precession states. If observed experimentally these could become a strong argument in favor of the spin-transfer theory in the present form.

Our method is fairly general and can be used to calculate exact switching diagrams for devices with new anisotropy patterns as they will be fabricated for future experiments. Although it does not give a complete picture (no information about the stable cycles far away from equilibrium points can be obtained), it is still very useful to develop an understand-

ing of the current-induced magnetic switching.

For example, since up to date magnetization direction is not experimentally measured but rather inferred from the resistive state of the wire, it is important and greatly simplifies comparison between theory and experiment that the number or resistive states can be different for axial and axis and plane cases due to the possibility of stabilizing the canted configuration. Also in these two cases the switching currents have qualitatively different dependence on the magnetic field. In experiments capable of direct measurement of \mathbf{M}_S one will see that it rotates by 180° degrees in the axial case and by a magnetic-field-dependent angle $\theta_C(\mathbf{B})$ in the axis and plane case. The precession state can be a good candidate for observation with the magnetic force microscope, especially since its frequency can be tuned by current.

To get an estimate of the switching current density we calculate critical ω_j for the axial easy plane case at $\omega_H = 0$ using Eq. (15) and converting to normal units using Eq. (5). We get

$$\omega_j = \alpha \frac{|\omega_K|}{g(P, 1)} \Rightarrow j = \alpha \left(\frac{e}{\hbar} \right) \frac{|K^{(intr)} - 4\pi M^2|}{g(P, 1)} L_S.$$

For a small piece with $L_S = 1$ nm, damping $\alpha = 0.05$, and 40% polarization degree one gets $j \approx 6.7 \times 10^7$ A/cm² using the values of $K^{(intr)}$ and M for cobalt.

Below we make several remarks on the issues that were postponed so far and will be left for the future work.

According to Slonczewski,²⁶ the spin-transfer effect can be described by an additional term in the Landau-Lifshitz equation representing the torque induced by the current. Therefore Ref. 26 and other papers, which follow this school of thought (including the present one), implicitly assume that the magnets are completely described by the possibly space- and time-dependent mean-field magnetization $\mathbf{M}(r, t)$, and the spin-transfer torque leads to a rotation of \mathbf{M} . Another point of view, expressed in particular in Refs. 1–3, 9, 10, 49, 50, is that the current creates spin-wave excitations in the magnetic piece (see Appendix D). In a previous calculation²⁷ we found that spin waves can be even induced in a bulk magnet by a large current density ($> 10^8$ A/cm²). The analysis of the spin-wave picture and its comparison with the coherent rotation picture is beyond the scope of the present paper, but is a necessary direction of future investigations.

As derived in Ref. 26, the torques acting on \mathbf{M}_S and \mathbf{M}_L are equal in absolute value, because of an implicit assumption $l_{sd} \rightarrow \infty$ made in the derivation. For a finite ratio d/l_{sd} , where d is the thickness of the normal spacer between the magnetic pieces, the torque acting on the piece which electrons cross first as they flow with the current will be smaller. To establish the interaction electrons have to spend time in both pieces. Those hitting the piece downstream are already polarized by the upstream piece. But the magnetization of the upstream piece itself can only be influenced by the electrons reflected back to it from the downstream piece, and those electrons have to travel twice more distance in the normal spacer. Since the polarization decays in the spacer, those electrons will induce a smaller torque. The small mag-

netic piece will be upstream or downstream depending on the current direction, thus the torque formula will change when the current direction changes. We neglect this effect which is reasonable in the limit $d/l_{sd} \rightarrow 0$.

Everywhere in the derivation we assumed the Gilbert damping coefficient α to be a constant. However even for bulk materials α can depend on the direction of \mathbf{n} (see discussion in Ref. 10). This is even more true in the layered materials with ferromagnet–normal metal boundaries, where the possibility of electrons entering and leaving the ferromagnet leads to additional damping.^{49,51–54} For our analysis this complication would mean that each equilibrium will be characterized by a separate value of α that will be a function of the relative angle between the polarizer and analyzer for this particular equilibrium. For example, the dependence of the \mathbf{n}_C equilibrium direction for the axis and plane case, Sec. IV, on the magnitude of external magnetic field will translate into the $\alpha_C(B)$ dependence. The displacement of this equilibrium due to the current was negligible and can be ignored for α as well. For the precession state one expects to be sensitive to α averaged over the cycle. We want to note that the calculation of enhanced damping and α angular dependence⁵³ was done in the zero-current state, while the calculation of spin-transfer torque did not take into account the motion of magnetization. A systematic investigation of the interplay between these two processes may reveal more subtleties.

In summary, we have calculated the dynamics of magnetization reversal in a nanowire, as functions of applied current and magnetic field. Magnetic switching, as per experiment, is the dominant behavior. Switching can also occur, we find, to a new canted phase. Precession regions are present in the parameter space. The case of easy plane perpendicular to current has a particularly rich phase diagram. Comparison with experimental results for anisotropies considered in this work shows considerable areas of agreement with our switching diagrams. Overall, we find that switching diagrams depend critically on the anisotropy type and on orientation of spin polarizer and magnetic field. In experiments with a different combination of these external controls the switching diagram can and should be recalculated using the method developed here. It will generally contain the same types of regions: stable parallel and antiparallel configurations, stable canted configurations, various regions of bistability, and precession regions.

Our analysis allows us to make some qualitative conclusions about the dynamics of magnetization switching. Magnetization reversal dynamics can be strongly affected by the presence of canted phases in the phase diagram, even if canting is not stable for a given current and magnetic field. Reversal processes can be complex, and the presence of unstable magnetic states has the potential to both speed up and slow down reversal times. This has the intriguing potential for canted states to be used to engineer optimal reversal times.

ACKNOWLEDGMENTS

The authors are grateful to J. Z. Sun and J. Slonczewski for stimulating discussions and to the Aspen Center of Phys-

ics for hospitality. Ya. B. B. acknowledges the support of the U.S. Department of Energy, Office of Science, under Contract No. W-31-109-ENG-38, B.A.J. acknowledges the support of DARPA-ARO, Contract No. DAAD19-01-C0060, and S.C.Z. was supported by NSF under Grant Nos. DMR-9814289 and the U.S. Department of Energy, Office of Basic Energy Sciences, under Contract No. DE-AC03-76SF00515.

APPENDIX A: CONSTRAINT ON THE WIRE RADIUS

To calculate the wire radius at which switching due to the induced circular (“Oersted”) magnetic field is replaced by the spin-transfer effect switching one would need a good theory of the former. To appreciate the difference between the mechanisms, recall that induced field switching always happens through an instability towards a nonuniform magnetic configuration because a circular magnetic field would have no effect on the monodomain magnetic section of a circular wire.

For a very rough estimate we argue as follows. The magnetic field created by the current on the surface of a wire of radius R is $B \approx jR/c$, where j is the current density. It creates a $\mathbf{M} \times \mathbf{B}$ torque per unit volume. We estimate $M \approx \mu_B/a^3$, where a is the lattice constant and take the maximum possible value of the torque T_H associated with induced field:

$$\frac{T_H}{V} = \frac{\mu_B}{a^3} \frac{jR}{c}.$$

The maximum value of the spin-transfer torque can be estimated as $T_{ST} \approx \hbar I/e$ where I is the total current. Since $I = \pi R^2 L j$, where L is the length of the magnetic piece,

$$\frac{T_{ST}}{V} = \hbar \frac{j}{eL}$$

and the condition $T_{ST} \gg T_H$ leads to

$$R \ll \frac{a^3}{r_0 L},$$

$$r_0 = mc^2/e^2 \approx 10^{-15} \text{ m}$$

(r_0 is sometimes called a “classical radius of an electron.”) Now for $a \approx 3 \text{ \AA}$ and $L \approx 5 \text{ nm}$ we get $R \ll 1 \text{ \mu m}$, as the wire radius below which spin-transfer torques should dominate.

APPENDIX B: DEFINITION OF VECTORS AND DERIVATION OF THE EQUATION OF MOTION IN THE (ϕ, θ) COORDINATES.

To transform the vector equation (4) into a system of equations on (ϕ, θ) we introduce two vectors orthogonal to \mathbf{n} and parallel to the surface of the sphere (see Fig. 13):

$$\mathbf{e}_\phi = \frac{[\mathbf{e}_z \times \mathbf{n}]}{\sin \theta},$$

$$\mathbf{e}_\theta = [\mathbf{n} \times \mathbf{e}_\phi] = \mathbf{e}_z - \mathbf{n} \cos \theta \sin \theta.$$

This gives

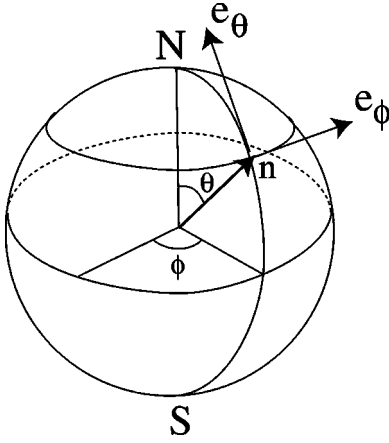


FIG. 13. Polar angles (ϕ, θ) and vectors \mathbf{e}_ϕ , \mathbf{e}_θ , and \mathbf{n} on the unit sphere.

$$\mathbf{e}_\phi = \{-\sin \phi, \cos \phi, 0\} = \frac{1}{\sin \theta} \{-n_y, n_x, 0\},$$

$$\mathbf{e}_\theta = \{-\cos \theta \cos \phi, -\cos \theta \sin \phi, \sin \theta\}.$$

For \mathbf{n} itself one has

$$\mathbf{n} = \{n_x, n_y, n_z\} = \{\sin \theta \cos \phi, \sin \theta \sin \phi, \cos \theta\}.$$

From there

$$[\mathbf{e}_\theta \times \mathbf{e}_\phi] = \mathbf{n},$$

$$[\mathbf{n} \times \mathbf{e}_\phi] = -\mathbf{e}_\theta,$$

$$[\mathbf{e}_\theta \times \mathbf{n}] = -\mathbf{e}_\phi,$$

and

$$\dot{\mathbf{e}}_\theta = -\dot{\theta} \mathbf{e}_r + \dot{\phi} \cos \theta \mathbf{e}_\phi,$$

$$\dot{\mathbf{e}}_\phi = -\dot{\phi} (\sin \theta \mathbf{e}_r + \cos \theta \mathbf{e}_\theta),$$

$$\dot{\mathbf{n}} = \dot{\theta} \mathbf{e}_\theta + \dot{\phi} \sin \theta \mathbf{e}_\phi.$$

More useful relationships follow

$$[\mathbf{n} \times \dot{\mathbf{n}}] = \dot{\theta} \mathbf{e}_\phi \dot{\phi} \sin \theta \mathbf{e}_\theta,$$

$$[\mathbf{n} \times \mathbf{z}] = -\sin \theta \mathbf{e}_\phi.$$

Next, we derive the equation of motion in the (ϕ, θ) coordinates. The end of vector \mathbf{n} moves along the unit sphere. So we have $\dot{\mathbf{n}} \perp \mathbf{n}$ and $\mathbf{F} \perp \mathbf{n}$, and both $\dot{\mathbf{n}}$ and \mathbf{F} can be expanded as a linear combination of \mathbf{e}_ϕ and \mathbf{e}_θ . First

$$\mathbf{F} = v_\phi \mathbf{e}_\phi + v_\theta \mathbf{e}_\theta$$

with

$$v_\phi = (\mathbf{F} \cdot \mathbf{e}_\phi); \quad v_\theta = (\mathbf{F} \cdot \mathbf{e}_\theta)$$

and second, from Eq. (B1),

$$\dot{\mathbf{n}} = \dot{\phi} \sin \theta \mathbf{e}_\phi + \dot{\theta} \mathbf{e}_\theta.$$

We obtain

$$[\mathbf{n} \times \dot{\mathbf{n}}] = \dot{\theta} \mathbf{e}_\phi + \dot{\phi} \sin \theta \mathbf{e}_\theta$$

so

$$\dot{\mathbf{n}} - \alpha [\mathbf{n} \times \dot{\mathbf{n}}] = \{\mathbf{e}_\phi, \mathbf{e}_\theta\} \begin{bmatrix} \sin \theta & -\alpha \\ -\alpha \sin \theta & -1 \end{bmatrix} \begin{Bmatrix} \dot{\phi} \\ \dot{\theta} \end{Bmatrix}$$

and Eq. (6) transforms to

$$\begin{bmatrix} \sin \theta & -\alpha \\ -\alpha \sin \theta & -1 \end{bmatrix} \begin{Bmatrix} \dot{\phi} \\ \dot{\theta} \end{Bmatrix} = \begin{Bmatrix} v_\phi \\ v_\theta \end{Bmatrix}. \quad (\text{B1})$$

APPENDIX C: DETAILS OF PRECESSION CALCULATIONS IN THE AXIAL CASE

To consider the properties of this quadratic equation

$$\frac{\omega_j \omega_K}{\alpha f(P)} = -\omega(\omega - \omega_H + \xi \omega_K)$$

let us look at a graph (Fig. 14). With $(\omega_j \omega_K)/(\alpha f) \equiv i$ plotted along the horizontal axis and ω plotted along the vertical axis, the graph is a parabola rotated by 90° . It crosses the vertical line $i=0$ at the points $\omega_1=0$ and $\omega_2 = h \xi \omega_K$. The vertex of the parabola is located at $\omega_c = (\omega_H - \xi \omega_K)/2$, $i_c = -\omega_c(\omega_c - \omega_H + \xi \omega_K) = (\omega_H \xi \omega_K)^2/4$.

We see that in general Eq. (23) has two solutions for $i \leq i_c$ and zero solutions otherwise. However if Eq. (21) has to be satisfied, there may be values of $i \leq i_c$, for which there is only one acceptable solution. The number of acceptable solutions depends on the position of the parabola vertex. If ω_c lies between ω_- and ω_+ , there are at least some values of i with two solutions. Otherwise, there is only one acceptable solution for all $i \leq i_c$. The intervals of i where solutions exist can be described as follows. There is one acceptable solution for

$$i(\omega_-) \leq i \leq i(\omega_+),$$

$$i(\omega) \equiv -\omega(\omega - \omega_H + \xi \omega_K),$$

and there are two solutions in the interval

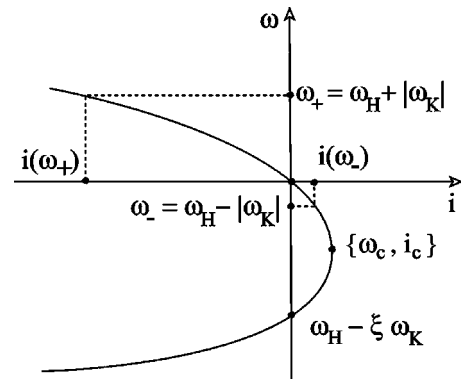


FIG. 14. Graphical solution of Eq. (23).

$$\max(i(\omega_-), i(\omega_+)) \leq i \leq i_c.$$

In the latter case there are two cycles, and it is possible to check that one is stable and the other is unstable. Using the formulas for ω_{\pm} and i_c we can now in principle plot the domains with one and two cycles on the (ω_j, ω_H) plane.

To see how those domains will fit in with the stability domains of the North and South Poles, we now establish a relationship between the values of $i(\omega_{\pm})$ and the stability boundaries of those equilibrium points. We have

$$\omega_{jN} = -\alpha \frac{\omega_H + \omega_K}{g(1)} = -\alpha(\omega_H + \omega_K)f(1 + \xi),$$

$$\omega_{jS} = -\alpha \frac{\omega_- - \omega_K}{g(-1)} = -\alpha(\omega_H - \omega_K)f(-1 + \xi),$$

therefore

$$i_N = -(\omega_H + \omega_K)\omega_K(1 + \xi),$$

$$i_S = -(\omega_H - \omega_K)\omega_K(-1 + \xi).$$

On the other hand

$$i(\omega_+) = -(\omega_H + |\omega_K|)(|\omega_K| + \xi\omega_K),$$

$$i(\omega_-) = -(\omega_H - |\omega_K|)(-|\omega_K| + \xi\omega_K),$$

which means that for $\omega_K > 0$

$$i(\omega_+) = i_N, \quad i(\omega_-) = i_S$$

and for $\omega_K < 0$

$$i(\omega_+) = i_S, \quad i(\omega_-) = i_N.$$

First, these relationships mean that there is one precession solution for i between i_N and i_S (depending on ω_K and ω_H one can have $i_N > i_S$ or $i_N < i_S$). Existence of a solution in this interval either means that a stable cycle exists between the poles when they are both unstable or an unstable cycle separates two stable poles. Second, for

$$\max(i_N, i_S) \leq i \leq i_c \quad (C1)$$

there are two cycles: one stable and one unstable. Since for those values of i only one of the poles is stable, the overall configuration is a stable cycle and a stable pole, separated by an unstable cycle. We will call this state a cycle-and-pole state, and denote it as PS+N or PS+S depending on which pole is stable.

Condition $\omega_- \leq \omega_c \leq \omega_+$ gives the interval of ω_H ,

$$\omega_{H1} \leq \omega_H \leq \omega_{H2}, \quad \omega_{H1} \equiv -\xi\omega_K - 2|\omega_K|,$$

$$\omega_{H2} \equiv -\xi\omega_K + 2|\omega_K|$$

for which the cycle-and-pole state exists. Note that the stability lines for the North and South Poles cross at the point $\omega_H = \omega_{Hc}$ given by the equation $\omega_{jN} = \omega_{jS}$ from which we get $\omega_{Hc} = -\xi\omega_K = (\omega_{H1} + \omega_{H2})/2$. So the region of existence of the cycle-and-pole state is symmetric with respect to ω_{Hc} . In the (ω_j, ω_H) switching diagram it lies next to the region

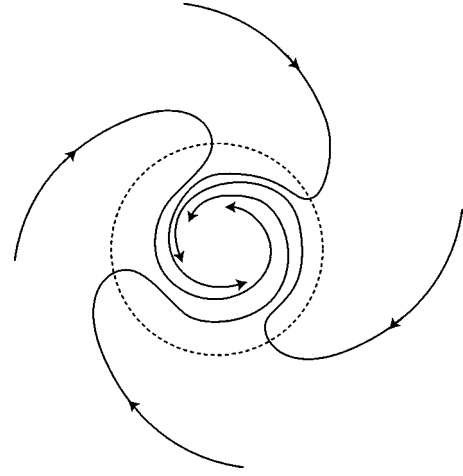


FIG. 15. Precession direction is reversed on the parallel with $\dot{\phi}=0$. This is an additional element of the time-evolution flow which must be taken into account when parallels with $\dot{\phi}=0$ and $\dot{\theta}=0$ do not coincide.

of stable North Pole for $\omega_K > 0$ and next to the region of the stable South Pole for $\omega_K < 0$ as shown in Fig. 3.

As current is swept through the precession region at constant ω_H , the frequency of the precession changes continuously and one can pose a question about the boundaries of the interval the frequency sweeps. Here we will discuss this question rather briefly. For those values of ω_H where the cycle-and-pole does not exist, the precession cycle is created near one of the poles and then moves towards the other, where it becomes the stable point. In this case the frequency changes in the interval $[\omega_-, \omega_+]$. If the cycle-and-pole exists, the stable cycle does not reach the other pole, but disappears due to mutual annihilation with an unstable cycle, which was created at the other pole and moved towards the stable cycle. The next step is to convince oneself that precession exists for $i(\omega_-) < i(\omega_+)$ and using Fig. 14 see that for increasing current the stable cycle is created at $i = i(\omega_-)$, then the unstable cycle is created at $i = i(\omega_+)$, and finally cycles merge and annihilate at $i = i_c$. The frequency of the stable cycle changes in the interval $[\omega_-, \omega_c]$. This picture shows that the boundary between PS region and the cycle-and-pole region happens when an unstable cycle is created. Consequently nothing happens there with the stable cycle and there is no singularity in $\omega(\omega_j)$ dependence when this line is crossed.

There is one final note about the properties of the time-evolution flow. In the discussion above we concentrated on finding the values of θ for which $\dot{\theta}=0$ and obtained stable and unstable cycles. However those values of θ for which $\dot{\phi}=0$ also play an important role in the shape of the phase flow; namely, at those lines the flow can change direction from clockwise to counterclockwise as shown in Fig. 15. In the absence of the current $\dot{\phi}=0$ and $\dot{\theta}=0$ lines coincide, but for nonzero current this is not true any more. One should always bear this peculiarity in mind while thinking about particular cases of phase flow.

APPENDIX D: SPIN-WAVE PICTURE

The idea about the possibility of spin-wave excitation first comes from considering current propagation through the normal-metal–ferromagnet boundary in the diffusive regime where the mean free path l of the electrons is much smaller than the spin-diffusion length l_{sd} . In this case the equilibration of electrons with the same spin happens much faster than equilibration between two different spin directions and a non-equilibrium state near the boundary can be described well by two chemical potentials⁵⁵ $\mu_{\uparrow}(r)$ and $\mu_{\downarrow}(r)$ of electrons with spins being parallel and antiparallel to the magnetization of the ferromagnet. When the current is passed, those two chemical potentials become different near the boundary (see Fig. 16). For example, when electrons flow from the normal metal into the ferromagnet, the energy of the spin-down electrons is larger than that of spin up. This is a non-equilibrium effect and $\mu_{\downarrow} - \mu_{\uparrow}$ is proportional to the current magnitude.

One can notice that this energy difference could be released if an additional mechanism of spin flipping would be provided. Spin-wave generation at the boundary is exactly such mechanism. An electron flips the spin from $-1/2$ to $+1/2$ and excites a magnon with $s = 1$, thus spin conservation is satisfied. Normally due to the anisotropies in the ferromagnet, the spin-wave spectrum has a gap Ω_0 ; so to satisfy the energy conservation one should increase current until $\mu_{\downarrow} - \mu_{\uparrow} \geq \Omega_0$ is true. This condition sets the current threshold for spin-wave generation. It was suggested^{1,25} that the resistivity jump observed in the experiment with current injection into a multilayer was the signature of reaching this threshold. There was however no clear understanding of either generation mechanism or the mechanism by which spin waves lead to a resistivity jump.

The fact that spin-wave generation is allowed by energy and spin conservation was emphasized very early by Berger.⁴⁹ The next (and not yet understood) question is the generation mechanism and the nature of the spin-wave state. In particular, it is not known whether the spin waves created will be coherent or incoherent. The coherent spin waves can be described with a time- and space-dependent magnetization $\mathbf{M}(r, t)$. This was first done by the authors²⁷ by deriving a continuous version of the modified Landau-Lifshitz equations and considering the effect of current on spin waves in the bulk ferromagnet (see also Ref. 34). For some special cases of multilayer structures this was done analytically³⁷ and numerically.^{35,36} In this approach it is still assumed that each electron interacts with the mean-field magnetization \mathbf{M} and only the cumulative effect of many electrons drives the

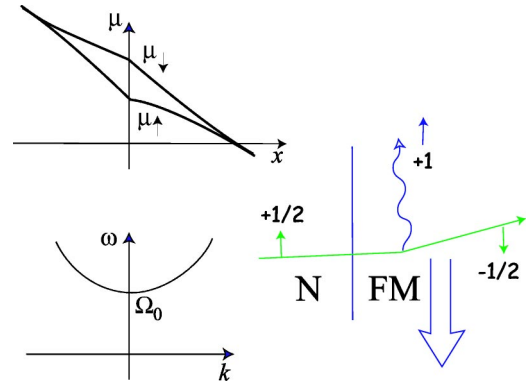


FIG. 16. (Color online) Left up: splitting chemical potentials near the normal metal–ferromagnet boundary with electric current flowing perpendicular to it. Left down: spectrum of spin waves in a ferromagnet with the uniaxial anisotropy. Right: spin conservation in the process of magnon emission.

wave. The precession states described in this paper are a particular case of coherent spin waves with no spatial dependence (or zero wave vector).

The incoherent spin waves are described not by $\mathbf{M}(r, t)$ but by a distribution function of magnons. The difference between them and coherent spin waves is analogous to the difference between the sound waves and the thermal phonons. Although both are associated with the same elastic properties of the solid, they represent different states of the solid body. For example, the incoherent thermal phonons do not create deformations. To have sound one needs a coherent superposition of many phonons in one state. Analogously, the presence of incoherent magnons does not create a precessing $\mathbf{M}(\mathbf{t})$ in the ferromagnet but rather decreases the magnitude of \mathbf{M} . In the incoherent picture each magnon is created by a spin flip of an individual electron (compare with the “magnon-assisted tunneling” picture⁵⁶), while in the coherent spin-wave picture many electrons are needed to drive the wave. In terms of influencing the current propagation, a state with incoherent magnons is also very different from a single coherent spin-wave state. Formally the influence of magnons appears as a change of a collision integral in the Boltzmann equation for electrons, while the single spin-wave influence modifies the electron motion between the collisions and appears as a change of the convective terms.

The questions about the mechanisms of spin-wave generation and about the nature of the spin wave state of the ferromagnetic pieces are very important but are not clearly understood at the present time, which calls for more work in future.

¹M. Tsoi, A.G.M. Jansen, J. Bass, W.-C. Chiang, M. Seck, V. Tsoi, and P. Wyder, Phys. Rev. Lett. **80**, 4281 (1998).

²M. Tsoi, A.G.M. Jansen, J. Bass, W.-C. Chiang, V. Tsoi, and P. Wyder, Nature (London) **406**, 46 (2000).

³M. Tsoi, V. Tsoi, J. Bass, A.G.M. Jansen, and P. Wyder, Phys. Rev. Lett. **89**, 246803 (2002).

⁴J.E. Wegrowe, D. Kelly, Y. Jaccard, Ph. Guittienne, and J.-Ph. Ansermet, Europhys. Lett. **45**, 626 (1999).

⁵Y. Jaccard, Ph. Guittienne, D. Kelly, J.-E. Wegrowe, and J.-Ph. Ansermet, Phys. Rev. B **62**, 1141 (2000).

⁶J.-E. Wegrowe, D. Kelly, T. Truong, P. Guittienne, and J.-P. Ansermet, Europhys. Lett. **56**, 748 (2001).

- ⁷J.-E. Wegrowe, X. Hoffer, Ph. Guittienne, A. Fabian, L. Gravier, T. Wade, and J.-Ph. Ansermet, *J. Appl. Phys.* **91**, 6806 (2002).
- ⁸J.-E. Wegrowe, A. Fabian, Ph. Guittienne, X. Hoffer, D. Kelly, J.-P. Ansermet, and E. Olive, *Appl. Phys. Lett.* **80**, 3775 (2002).
- ⁹E.B. Myers, D.C. Ralph, J.A. Katine, R.N. Louie, and R.A. Buhrman, *Science* **285**, 867 (1999).
- ¹⁰J.A. Katine, F.J. Albert, R.A. Buhrman, E.B. Myers, and D.C. Ralph, *Phys. Rev. Lett.* **84**, 3149 (2000).
- ¹¹F.J. Albert, J.A. Katine, R.A. Buhrman, and D.C. Ralph, *Appl. Phys. Lett.* **77**, 3809 (2000).
- ¹²F.J. Albert, N.C. Emley, E.B. Myers, D.C. Ralph, and R.A. Buhrman, *Phys. Rev. Lett.* **89**, 226802 (2002).
- ¹³E.B. Myers, F.J. Albert, J.C. Sankey, E. Bonet, R.A. Buhrman, and D.C. Ralph, *Phys. Rev. Lett.* **89**, 196801 (2002).
- ¹⁴J.Z. Sun, *J. Magn. Magn. Mater.* **202**, 157 (1999).
- ¹⁵J.Z. Sun, D.J. Monsma, D.W. Abraham, M.J. Rooks, and R.H. Koch, *Appl. Phys. Lett.* **81**, 2202 (2002).
- ¹⁶J. Grollier, V. Cros, A. Hamzic, J.M. George, H. Jaffres, A. Fert, G. Faini, J. Ben Youssef, and H. Legall, *Appl. Phys. Lett.* **78**, 3663 (2001).
- ¹⁷J. Grollier, V. Cros, H. Jaffres, A. Hamzic, J.M. George, G. Faini, J.B. Youssef, H. Le Gall, and A. Fert, *Phys. Rev. B* **67**, 174402 (2003).
- ¹⁸F.B. Mancoff and S.E. Russek, *IEEE Trans. Magn.* **38**, 2853 (2002).
- ¹⁹M.R. Pufall, W.H. Rippard, and T.J. Silva, *Appl. Phys. Lett.* **83**, 323 (2003).
- ²⁰W.H. Rippard, M.R. Pufall, and T.J. Silva, *Appl. Phys. Lett.* **82**, 1260 (2003).
- ²¹S. Urazhdin, Norman O. Birge, W.P. Pratt, Jr., and J. Bass, *Phys. Rev. Lett.* **91**, 146803 (2003).
- ²²S. Urazhdin, H. Kurt, W.P. Pratt, Jr., and J. Bass, *Appl. Phys. Lett.* **83**, 114 (2003).
- ²³S. Urazhdin, W.P. Pratt, Jr., and J. Bass, cond-mat/0304299 (unpublished).
- ²⁴Collection of articles in *IBM J. Res. Dev.* **42** (1998).
- ²⁵L. Berger, *Phys. Rev. B* **33**, 1572 (1986); *J. Appl. Phys.* **63**, 1663 (1988).
- ²⁶J. Slonczewski, *J. Magn. Magn. Mater.* **159**, L1 (1996); US Patent No. 5,695,864 (Dec. 9 1997).
- ²⁷Ya.B. Bazaliy, B.A. Jones, and Shoucheng Zhang, *Phys. Rev. B* **57**, R3213 (1998).
- ²⁸Ya.B. Bazaliy, B.A. Jones, and Shoucheng Zhang, cond-mat/0009034 (unpublished).
- ²⁹Ya.B. Bazaliy, B.A. Jones, and Shoucheng Zhang, *J. Appl. Phys.* **89**, 6793 (2001).
- ³⁰Ya.B. Bazaliy and B.A. Jones, *Physica B* **329-333**, 1290 (2003).
- ³¹J.Z. Sun, *Phys. Rev. B* **62**, 570 (2000).
- ³²J. Slonczewski, unpublished talks on many conferences, including APS 2000, EMMA2000, talks at IBM seminars, etc.
- ³³K. Bussman, G.A. Prinz, S.-F. Cheng, and D. Wang, *Appl. Phys. Lett.* **75**, 2476 (1999).
- ³⁴J. Fernandez-Rossier, M. Braun, and A. MacDonald, Abstracts of the 47th Conference on Magnetism and Magnetic Materials, Tampa, Florida, FD-14, 292, (2002) (unpublished).
- ³⁵J. Miltat, G. Albuquerque, A. Thiaville, and C. Vouille, *J. Appl. Phys.* **89**, 6982 (2001).
- ³⁶R. H. Koch (unpublished).
- ³⁷J. Slonczewski, *J. Magn. Magn. Mater.* **195**, L261 (1999).
- ³⁸L. D. Landau and E. M. Lifshitz, *Electrodynamics of Continuous Media* (Elsevier, Amsterdam, 1996), Sec. 45.
- ³⁹X. Waintal, E.B. Myers, P.W. Brouwer, and D.C. Ralph, *Phys. Rev. B* **62**, 12 317 (2000).
- ⁴⁰G.E.W. Bauer, Ya. Tserkovnyak, D. Huertas-Hernando, and A. Brataas, *Phys. Rev. B* **67**, 94 421 (2003).
- ⁴¹K. Xia, P.J. Kelly, G.E.W. Bauer, A. Brataas, and I. Turek, *Phys. Rev. B* **65**, 220401 (2002).
- ⁴²Al. Kovalev, A. Brataas, and G.E.W. Bauer, *Phys. Rev. B* **66**, 224424 (2002).
- ⁴³M.D. Stiles and A. Zangwill, *Phys. Rev. B* **66**, 014407 (2002); *J. Appl. Phys.* **91**, 6812 (2002).
- ⁴⁴C. Heide, *Phys. Rev. Lett.* **87**, 197201 (2001); *Phys. Rev. B* **65**, 054401 (2002).
- ⁴⁵S. Zhang, P.M. Levy, and A. Fert, *Phys. Rev. Lett.* **88**, 236601 (2002).
- ⁴⁶J.-L. Maurice, D. Imhoff, P. Etienne, O. Durand, S. Dubois, L. Piraux, J.-M. George, P. Galtier, and A. Fert, *J. Magn. Magn. Mater.* **184**, 1 (1998).
- ⁴⁷U. Ebels, A. Radulescu, Y. Henry, L. Piraux, and K. Ounadjela, *Phys. Rev. Lett.* **84**, 983 (2000).
- ⁴⁸F. Albert (private communication).
- ⁴⁹L. Berger, *Phys. Rev. B* **33**, 1572 (1986); **54**, 9353 (1996); *J. Appl. Phys.* **81**, 4880 (1997); *IEEE Trans. Magn.* **34**, 3837 (1998).
- ⁵⁰M.V. Tsoi and V.S. Tsoi, *JETP Lett.* **73**, 98 (2001).
- ⁵¹P. Monod, H. Hurdequint, A. Janossy, J. Obert, and J. Chaumont, *Phys. Rev. Lett.* **29**, 1327 (1972); H. Hurdequint and G. Dunifer, *J. Phys. (Paris), Colloq.* **49**, C8-1717 (1988); H. Hurdequint, *J. Magn. Magn. Mater.* **93**, 336 (1991).
- ⁵²L. Berger, *J. Appl. Phys.* **90**, 4632 (2001).
- ⁵³Y. Tserkovnyak, A. Brataas, and G.E.W. Bauer, *Phys. Rev. Lett.* **88**, 117601 (2002); *Phys. Rev. B* **66**, 224403 (2002).
- ⁵⁴B. Heinrich, Y. Tserkovnyak, G. Woltersdorf, A. Brataas, R. Urban, and G.E.W. Bauer, *Phys. Rev. Lett.* **90**, 187601 (2003).
- ⁵⁵P.C. van Son, H. van Kempen, and P. Wyder, *Phys. Rev. Lett.* **58**, 2271 (1987).
- ⁵⁶E. McCann and V.I. Fal'ko, *Appl. Phys. Lett.* **81**, 3609 (2002).